

Fermion pair production at e^-e^+ linear collider experiments in GUT inspired gauge-Higgs unification

Shuichiro Funatsu¹, Hisaki Hatanaka², Yutaka Hosotani³,
Yuta Orikasa⁴ and Naoki Yamatsu⁵

¹*Institute of Particle Physics and Key Laboratory of Quark and Lepton Physics (MOE),
Central China Normal University, Wuhan, Hubei 430079, China*

²*Osaka, Osaka 536-0014, Japan*

³*Department of Physics, Osaka University, Toyonaka, Osaka 560-0043, Japan*

⁴*Institute of Experimental and Applied Physics, Czech Technical University in Prague,
Husova 240/5, 110 00 Prague 1, Czech Republic*

⁵*Department of Physics, Kyushu University, Fukuoka 819-0395, Japan*

Abstract

Fermion pair production at e^-e^+ linear collider experiments with polarized e^- and e^+ beams is examined in the GUT inspired $SO(5) \times U(1) \times SU(3)$ gauge-Higgs unification. There arises large parity violation in the couplings of leptons and quarks to Kaluza-Klein (KK) excited neutral vector bosons Z' s, which leads to distinctive polarization dependence in cross sections, forward-backward asymmetries, left-right asymmetries, and left-right forward-backward asymmetries in various processes. Those effects are detectable even for the KK mass scale up to about 15 TeV at future e^-e^+ linear collider experiments with energies 250 GeV to 1 TeV.

1 Introduction

The standard model (SM) in particle physics has been established at low energies. However, it is not yet clear that the observed Higgs boson has exactly the same properties as those in the SM. It is necessary to determine the Higgs couplings to quarks, leptons, SM gauge bosons, and the Higgs self-couplings with better accuracy in future experiments.

There remain uneasy points in the Higgs boson sector in the SM. While the dynamics of the SM gauge bosons, the photon, W and Z bosons and gluons is governed by the gauge principle, dynamics of the Higgs boson in the SM is not. Higgs couplings of quarks and leptons as well as Higgs self-couplings are not regulated by any principle. At the quantum level, there arise huge corrections to the Higgs boson mass, which have to be canceled and tuned by hand to obtain the observed 125 GeV mass. One way to achieve the stabilization of the Higgs boson mass against quantum corrections is to identify the Higgs boson with the zero mode of the fifth dimensional component of the gauge potential [1–6]. This scenario is referred to as gauge-Higgs unification (GHU).

In GHU the Higgs field appears as a fluctuation mode of the Aharonov-Bohm (AB) phase θ_H in the fifth dimension. The $SU(3)_C \times SO(5) \times U(1)_X$ gauge theory in the Randall-Sundrum (RS) warped space has been proposed in Refs. [7–15]. It gives nearly the same phenomenology at low energies as the SM [10–12, 16]. Deviations of the gauge couplings of quarks and leptons from the SM values are less than 0.1% for $\theta_H \simeq 0.1$. Higgs couplings of quarks, leptons, W and Z bosons are approximately the SM values times $\cos \theta_H$; the deviation is about 1%. In one type of the models the Kaluza-Klein (KK) mass scale turns out about $m_{\text{KK}} \simeq 8 \text{ TeV}$ for $\theta_H \simeq 0.1$. KK excited states contribute in intermediate states of the two γ decay of the Higgs boson. Their contribution is finite and very small. The signal strengths of various Higgs decay modes are approximately $\cos^2 \theta_H$ times the SM values. The branching fractions of those decay modes are approximately the same as in the SM.

GHU predicts Z' bosons, which are the KK modes of γ , Z , and Z_R . They are mixed vector bosons of $U(1)_X$, $U(1)_L \subset SU(2)_L$, and $U(1)_R \subset SU(2)_R$ where $SU(2)_L \times SU(2)_R \subset SO(5)$. In the model with quark-lepton multiplets introduced in the vector representation of $SO(5)$, which is referred to as the *A-model* below, masses of Z' bosons are in the 6 TeV–9 TeV range for $\theta_H = 0.11$ –0.07. They have broad widths and can be produced at 14 TeV Large Hadron Collider (LHC). The current non-observation of Z' signals puts the limit $\theta_H \lesssim 0.11$. Distinct signals of the gauge-Higgs unification can be found in e^-e^+ collisions [17–21]. Large parity violation appears in the couplings of quarks and leptons to KK gauge bosons, particularly to the Z' bosons. In the A-model, right-handed

quarks and charged leptons have rather large couplings to Z' bosons. The interference effects of Z' bosons can be clearly observed at 250 GeV e^-e^+ International Linear Collider (ILC) [22–28]. In the process $e^-e^+ \rightarrow \mu^-\mu^+$, the deviation from the SM amounts to -4% with the electron beam polarized in the right-handed mode by 80% ($P_{e^-} = 0.8$) for $\theta_H \simeq 0.09$, whereas there appears negligible deviation with the electron beam polarized in the left-handed mode by 80% ($P_{e^-} = -0.8$). In the forward-backward asymmetry $A_{FB}(e^-e^+ \rightarrow \mu^-\mu^+)$ the deviation from the SM becomes -2% for $P_{e^-} = 0.8$. These deviations can be seen at 250 GeV ILC even with 250fb^{-1} data [22–28]. We note that the ILC designs 80% polarization of the electron beam and 30% polarization of the positron beam according to the ILC Technical Design Report [29–33]. The significance of polarized positrons and electrons for several new physics searches at the ILC is summarized in Ref. [34].

Recently, an alternative gauge-Higgs unification model with quark-lepton multiplets introduced in the spinor, vector, and singlet representations of $SO(5)$, which is referred to as the *B-model* below, has been proposed [13]. The B-model can be embedded in the $SO(11)$ gauge-Higgs grand unification [35–42], where the SM gauge group and quark-lepton content are incorporated into grand unified theory (GUT) [43–48] in higher dimensional framework [49–59].

In this paper, we evaluate cross sections, forward-backward asymmetries [60, 61], left-right asymmetries [60–63], and left-right forward-backward asymmetries [61, 64–67] in the processes $e^-e^+ \rightarrow f\bar{f}$ ($f\bar{f} = \mu^-\mu^+, c\bar{c}, b\bar{b}, t\bar{t}$) in the GUT inspired GHU, the B-model. The quantities in the process $e^-e^+ \rightarrow \tau^-\tau^+$ are almost the same as in the process $e^-e^+ \rightarrow \mu^-\mu^+$, as the couplings of τ^\pm to Z' 's are nearly the same as those of μ^\pm . For the process $e^-e^+ \rightarrow e^-e^+$ there is an additional contribution from the BhaBha scattering [23, 34, 68–71], the analysis of which is given separately. We shall find a significant difference between predictions from the SM and those from the B-model at e^-e^+ linear collider experiments with polarized beams.

Z' bosons appear in many models beyond the SM and various physical consequences have been examined [72–74]. In most cases couplings of Z' bosons to quarks and leptons are comparable to those of Z boson. The situation is quite different in GHU. As was shown in the A-model in Ref. [17] and is shown below in the B-model, either left-handed or right-handed components of quarks and leptons have rather large couplings to Z' bosons, particularly to the first KK modes of γ , Z and Z_R . We shall see that substantial deviations from the SM can be seen in cross sections and other quantities in $e^-e^+ \rightarrow f\bar{f}$ processes at ILC even though those Z' bosons may be as heavy as 10 TeV.

There are similarities between composite Higgs models [7, 75–78] and GHU models. The Higgs boson appears as a pseudo-Nambu-Goldstone boson in composite Higgs models whereas it appears as an AB phase in the fifth dimension in GHU models. The Higgs boson has a character of a phase in both models and the couplings of the Higgs boson exhibit qualitatively similar behavior. Z' bosons appear KK modes of neutral gauge bosons in GHU models whose couplings to quarks and leptons are unambiguously determined once the models are specified. Analogues of Z' bosons in the composite Higgs model are composite vector bosons [79]. It is interesting to explore implications of those composite vector bosons in e^-e^+ collisions.

The paper is organized as follows. In Sec. 2, the model is introduced. In Sec. 3, we quickly review the definition of observables such as cross sections, forward-backward asymmetries, left-right asymmetries, and left-right forward-backward asymmetries. In Sec. 4, we evaluate cross sections and other observables in $e^-e^+ \rightarrow f\bar{f}$ with $f\bar{f} = \mu^-\mu^+$, $c\bar{c}$, $b\bar{b}$, and $t\bar{t}$. Section 5 is devoted to summary and discussions. Useful formulas for decay widths are given in Appendix A.

2 Model

The GUT inspired $SU(3)_C \times SO(5) \times U(1)_X$ GHU model has been introduced in Ref. [13] and further investigated in Refs. [14, 15]. It is defined in the RS warped space with metric given by

$$ds^2 = g_{MN}dx^M dx^N = e^{-2\sigma(y)}\eta_{\mu\nu}dx^\mu dx^\nu + dy^2, \quad (2.1)$$

where $M, N = 0, 1, 2, 3, 5$, $\mu, \nu = 0, 1, 2, 3$, $y = x^5$, $\eta_{\mu\nu} = \text{diag}(-1, +1, +1, +1)$, $\sigma(y) = \sigma(y + 2L) = \sigma(-y)$, and $\sigma(y) = ky$ for $0 \leq y \leq L$. In terms of the conformal coordinate $z = e^{ky}$ ($1 \leq z \leq z_L = e^{kL}$) in the region $0 \leq y \leq L$

$$ds^2 = \frac{1}{z^2} \left(\eta_{\mu\nu}dx^\mu dx^\nu + \frac{dz^2}{k^2} \right). \quad (2.2)$$

The bulk region $0 < y < L$ ($1 < z < z_L$) is anti-de Sitter (AdS) spacetime with a cosmological constant $\Lambda = -6k^2$, which is sandwiched by the UV brane at $y = 0$ ($z = 1$) and the IR brane at $y = L$ ($z = z_L$). The KK mass scale is $m_{\text{KK}} = \pi k/(z_L - 1) \simeq \pi k z_L^{-1}$ for $z_L \gg 1$.

Let us denote gauge fields of $SU(3)_C$, $SO(5)$, and $U(1)_X$ by $A_M^{SU(3)_C}$, $A_M^{SO(5)}$, and $A_M^{U(1)_X}$, respectively. The orbifold boundary conditions (BCs) are given by

$$\begin{pmatrix} A_\mu \\ A_y \end{pmatrix} (x, y_j - y) = P_j \begin{pmatrix} A_\mu \\ -A_y \end{pmatrix} (x, y_j + y) P_j^{-1} \quad (2.3)$$

for each gauge field, where $(y_0, y_1) = (0, L)$. In terms of

$$P_{\mathbf{3}}^{SU(3)} = I_3, \quad P_{\mathbf{4}}^{SO(5)} = \text{diag}(I_2, -I_2), \quad P_{\mathbf{5}}^{SO(5)} = \text{diag}(I_4, -I_1), \quad (2.4)$$

$P_0 = P_1 = P_{\mathbf{3}}^{SU(3)}$ for $A_M^{SU(3)C}$ and $P_0 = P_1 = 1$ for $A_M^{U(1)X}$. $P_0 = P_1 = P_{\mathbf{5}}^{SO(5)}$ for $A_M^{SO(5)}$ in the vector representation and $P_{\mathbf{4}}^{SO(5)}$ in the spinor representation, respectively. The orbifold BCs $P_{\mathbf{4}}^{SO(5)}$ and $P_{\mathbf{5}}^{SO(5)}$ break $SO(5)$ to $SO(4) \simeq SU(2)_L \times SU(2)_R$. W, Z bosons and γ (photon) are zero modes in the $SO(4)$ part of $A_\mu^{SO(5)}$, whereas the 4D Higgs boson is a zero mode in the $SO(5)/SO(4)$ part of $A_y^{SO(5)}$. In the GHU model, extra neutral gauge bosons Z' correspond to KK photons $\gamma^{(n)}$, KK Z bosons $Z^{(n)}$, and KK Z_R bosons $Z_R^{(n)}$ ($n \geq 1$), where the γ , and Z, Z_R bosons are the mass eigen states of the electro-magnetic $U(1)_{\text{EM}}$ neutral gauge bosons of $SU(2)_L, SU(2)_R$, and $U(1)_X$.

Matter fields are introduced both in the 5D bulk and on the UV brane. They are listed in Table 1. The SM quark and lepton multiples are identified with the zero modes of the quark and lepton multiplets $\Psi_{(\mathbf{3},\mathbf{4})}^\alpha$ ($\alpha = 1, 2, 3$), $\Psi_{(\mathbf{3},\mathbf{1})}^{\pm\alpha}$, and $\Psi_{(\mathbf{1},\mathbf{4})}^\alpha$ in Table 2. These fields obey the following BCs:

$$\begin{aligned} \Psi_{(\mathbf{3},\mathbf{4})}^\alpha(x, y_j - y) &= -P_{\mathbf{4}}^{SO(5)} \gamma^5 \Psi_{(\mathbf{3},\mathbf{4})}^\alpha(x, y_j + y), \\ \Psi_{(\mathbf{3},\mathbf{1})}^{\pm\alpha}(x, y_j - y) &= \mp \gamma^5 \Psi_{(\mathbf{3},\mathbf{1})}^{\pm\alpha}(x, y_j + y), \\ \Psi_{(\mathbf{1},\mathbf{4})}^\alpha(x, y_j - y) &= -P_{\mathbf{4}}^{SO(5)} \gamma^5 \Psi_{(\mathbf{1},\mathbf{4})}^\alpha(x, y_j + y). \end{aligned} \quad (2.5)$$

With BCs (2.5), the parity assignment of quarks and leptons are summarized in Table 2. (See Refs. [13–15] in detail.)

	B-model	A-model
Quark	$(\mathbf{3}, \mathbf{4})_{\frac{1}{6}} \quad (\mathbf{3}, \mathbf{1})_{-\frac{1}{3}}^+ \quad (\mathbf{3}, \mathbf{1})_{-\frac{1}{3}}^-$	$(\mathbf{3}, \mathbf{5})_{\frac{2}{3}} \quad (\mathbf{3}, \mathbf{5})_{-\frac{1}{3}}$
Lepton	$(\mathbf{1}, \mathbf{4})_{-\frac{1}{2}}$	$(\mathbf{1}, \mathbf{5})_0 \quad (\mathbf{1}, \mathbf{5})_{-1}$
Dark fermion	$(\mathbf{3}, \mathbf{4})_{\frac{1}{6}} \quad (\mathbf{1}, \mathbf{5})_0^+ \quad (\mathbf{1}, \mathbf{5})_0^-$	$(\mathbf{1}, \mathbf{4})_{\frac{1}{2}}$
Brane fermion	$(\mathbf{1}, \mathbf{1})_0$	$(\mathbf{3}, [\mathbf{2}, \mathbf{1}])_{\frac{7}{6}, \frac{1}{6}, -\frac{5}{6}} \quad (\mathbf{1}, [\mathbf{2}, \mathbf{1}])_{\frac{1}{2}, -\frac{1}{2}, -\frac{3}{2}}$
Brane scalar	$(\mathbf{1}, \mathbf{4})_{\frac{1}{2}}$	$(\mathbf{1}, [\mathbf{1}, \mathbf{2}])_{\frac{1}{2}}$

Table 1: The $SU(3)_C \times SO(5) \times U(1)_X$ content of matter fields is shown in the GUT inspired model (B-model) and the previous model (A-model). The B-model is analyzed in the present paper.

The brane scalar field $\Phi_{(\mathbf{1},\mathbf{4})}(x)$ in Table 1 is responsible for breaking $SO(5) \times U(1)_X$ to $SU(2)_L \times U(1)_Y$. A spinor $\mathbf{4}$ of $SO(5)$ is decomposed into $[\mathbf{2}, \mathbf{1}] \oplus [\mathbf{1}, \mathbf{2}]$ of $SO(4) \simeq SU(2)_L \times SU(2)_R$. The $\Phi_{(\mathbf{1},\mathbf{4})}$ develops a nonvanishing vacuum expectation value (VEV):

$$\Phi_{(\mathbf{1},\mathbf{4})} = \begin{pmatrix} \Phi_{[\mathbf{2},\mathbf{1}]} \\ \Phi_{[\mathbf{1},\mathbf{2}]} \end{pmatrix}, \quad \langle \Phi_{[\mathbf{1},\mathbf{2}]} \rangle = \begin{pmatrix} 0 \\ w \end{pmatrix}, \quad (2.6)$$

Field	$(SU(3)_C \times SO(5))_X$	G_{22}	Left-handed	Right-handed	Name
$\Psi_{(3,4)}^\alpha$	$(\mathbf{3}, \mathbf{4})_{\frac{1}{6}}$	$[\mathbf{2}, \mathbf{1}]$	$(+, +)$	$(-, -)$	$\begin{matrix} u & c & t \\ d & s & b \end{matrix}$
		$[\mathbf{1}, \mathbf{2}]$	$(-, -)$	$(+, +)$	$\begin{matrix} u' & c' & t' \\ d' & s' & b' \end{matrix}$
$\Psi_{(3,1)}^{\pm\alpha}$	$(\mathbf{3}, \mathbf{1})_{-\frac{1}{3}}$	$[\mathbf{1}, \mathbf{1}]$	(\pm, \pm)	(\mp, \mp)	$D_d^\pm \ D_s^\pm \ D_b^\pm$
$\Psi_{(1,4)}^\alpha$	$(\mathbf{1}, \mathbf{4})_{-\frac{1}{2}}$	$[\mathbf{2}, \mathbf{1}]$	$(+, +)$	$(-, -)$	$\begin{matrix} \nu_e & \nu_\mu & \nu_\tau \\ e & \mu & \tau \end{matrix}$
		$[\mathbf{1}, \mathbf{2}]$	$(-, -)$	$(+, +)$	$\begin{matrix} \nu'_e & \nu'_\mu & \nu'_\tau \\ e' & \mu' & \tau' \end{matrix}$

Table 2: Parity assignment (P_0, P_1) of quark and lepton multiplets in the bulk is shown. G_{22} stands for $SU(2)_L \times SU(2)_R (\subset SO(5))$.

which reduces the symmetry $SU(3)_C \times SO(4) \times U(1)_X$ to the SM gauge group $G_{\text{SM}} \equiv SU(3)_C \times SU(2)_L \times U(1)_Y$. It is assumed that $w \gg m_{\text{KK}}$, which ensures that orbifold BCs for the 4D components of gauge fields corresponding to broken generators in the breaking $SU(2)_R \times U(1)_X \rightarrow U(1)_Y$ obey effectively Dirichlet conditions at the UV brane for low-lying KK modes [37]. Accordingly the mass of the neutral physical mode of $\Phi_{(1,4)}$ is much larger than m_{KK} .

The $U(1)_Y$ gauge boson is a mixed state of $U(1)_R (\subset SU(2)_R)$ and $U(1)_X$ gauge bosons. The $U(1)_Y$ gauge field B_M^Y is given in terms of the $SU(2)_R$ gauge fields $A_M^{a_R}$ ($a_R = 1_R, 2_R, 3_R$) and the $U(1)_X$ gauge field B_M by

$$B_M^Y = s_\phi A_M^{3_R} + c_\phi B_M. \quad (2.7)$$

Here the mixing angle ϕ between $U(1)_R$ and $U(1)_X$ is given by $c_\phi = \cos \phi \equiv g_A / \sqrt{g_A^2 + g_B^2}$ and $s_\phi = \sin \phi \equiv g_B / \sqrt{g_A^2 + g_B^2}$ where g_A and g_B are gauge couplings in $SO(5)$ and $U(1)_X$, respectively. The 4D $SU(2)_L$ gauge coupling is given by $g_w = g_A / \sqrt{L}$. The 5D gauge coupling g_Y^{5D} of $U(1)_Y$ and the 4D bare Weinberg angle at the tree level, θ_W^0 , are given by

$$g_Y^{5D} = \frac{g_A g_B}{\sqrt{g_A^2 + g_B^2}}, \quad \sin \theta_W^0 = \frac{s_\phi}{\sqrt{1 + s_\phi^2}}. \quad (2.8)$$

The 4D Higgs boson doublet $\phi_H(x)$ is the zero mode contained in the $A_z = (kz)^{-1} A_y$ component:

$$A_z^{(j5)}(x, z) = \frac{1}{\sqrt{k}} \phi_j(x) u_H(z) + \dots, \quad u_H(z) = \sqrt{\frac{2}{z_L^2 - 1}} z, \\ \phi_H(x) = \frac{1}{\sqrt{2}} \begin{pmatrix} \phi_2 + i\phi_1 \\ \phi_4 - i\phi_3 \end{pmatrix}. \quad (2.9)$$

Without loss of generality, we assume $\langle \phi_1 \rangle, \langle \phi_2 \rangle, \langle \phi_3 \rangle = 0$ and $\langle \phi_4 \rangle \neq 0$, which is related to the Aharonov-Bohm (AB) phase θ_H in the fifth dimension by $\langle \phi_4 \rangle = \theta_H f_H$, where

$$f_H = \frac{2}{g_w} \sqrt{\frac{k}{L(z_L^2 - 1)}}. \quad (2.10)$$

The gauge symmetry breaking pattern of $SU(3)_C \times SO(5) \times U(1)_X$ is given as

$$\begin{aligned} & SU(3)_C \times SO(5) \times U(1)_X \\ & \xrightarrow{BC} SU(3)_C \times SU(2)_L \times SU(2)_R \times U(1)_X \quad \text{at } y = 0, L \\ & \xrightarrow{\langle \Phi \rangle} SU(3)_C \times SU(2)_L \times U(1)_Y \quad \text{by the VEV } \langle \Phi_{(1,4)} \rangle \neq 0 \text{ at } y = 0 \\ & \xrightarrow{\theta_H} SU(3)_C \times U(1)_{EM} \quad \text{by the Hosotani mechanism,} \end{aligned} \quad (2.11)$$

where BC stands for orbifold boundary conditions.

3 Observables

Here we summarize formulas of several observables in the s -channel scattering processes of $e^-e^+ \rightarrow f\bar{f}$ mediated by only neutral vector bosons V_i such as γ and Z where $f\bar{f} \neq e^-e^+$. For $e^-e^+ \rightarrow e^-e^+$, there are contributions not only from the s -channel scattering process but also from the t -channel scattering process. The formulas given in this section must be modified when the intermediate state of the s -channel scattering process contains scalar fields. In GHU Z' bosons, $\gamma^{(n)}$, $Z^{(n)}$ and $Z_R^{(n)}$ ($n \geq 1$), give additional contributions to the $e^-e^+ \rightarrow f\bar{f}$ processes, which can be observed in future e^-e^+ collider experiments.

3.1 Cross section

The differential cross section for the $e^-e^+ \rightarrow f\bar{f}$ process is given by

$$\begin{aligned} & \frac{d\sigma^{f\bar{f}}}{d\cos\theta}(P_{e^-}, P_{e^+}, \cos\theta) \\ & = (1 - P_{e^-}P_{e^+}) \frac{1}{4} \left\{ (1 - P_{\text{eff}}) \frac{d\sigma_{LR}^{f\bar{f}}}{d\cos\theta}(\cos\theta) + (1 + P_{\text{eff}}) \frac{d\sigma_{RL}^{f\bar{f}}}{d\cos\theta}(\cos\theta) \right\} \end{aligned} \quad (3.1)$$

where P_{e^\pm} denotes longitudinal polarization of e^\pm . $P_{e^\pm} = +1$ corresponds to purely right-handed e^\pm . P_{eff} is defined as

$$P_{\text{eff}} \equiv \frac{P_{e^-} - P_{e^+}}{1 - P_{e^-}P_{e^+}}. \quad (3.2)$$

$d\sigma_{LR}/d\cos\theta$ and $d\sigma_{RL}/d\cos\theta$ are differential cross sections for $e_L^-e_R^+ \rightarrow f\bar{f}$ and $e_R^-e_L^+ \rightarrow f\bar{f}$:

$$\frac{d\sigma_{LR}^{f\bar{f}}}{d\cos\theta}(\cos\theta) = \frac{\beta_s}{32\pi} \left\{ [1 + \beta^2 \cos^2\theta] \{ |Q_{e_L f_L}|^2 + |Q_{e_L f_R}|^2 \} \right.$$

$$\begin{aligned}
& + 2\beta \cos \theta \left\{ |Q_{e_L f_L}|^2 - |Q_{e_L f_R}|^2 \right\} + 8 \frac{m_f^2}{s} \left[\text{Re}(Q_{e_L f_L} Q_{e_L f_R}^*) \right] \Big\}, \\
\frac{d\sigma_{RL}^{f\bar{f}}}{d\cos\theta}(\cos\theta) = & \frac{\beta s}{32\pi} \left\{ [1 + \beta^2 \cos^2 \theta] \left\{ |Q_{e_R f_R}|^2 + |Q_{e_R f_L}|^2 \right\} \right. \\
& \left. + 2\beta \cos \theta \left\{ |Q_{e_R f_R}|^2 - |Q_{e_R f_L}|^2 \right\} + 8 \frac{m_f^2}{s} \left[\text{Re}(Q_{e_R f_L} Q_{e_R f_R}^*) \right] \right\}, \tag{3.3}
\end{aligned}$$

where s is the square of the center-of-mass energy, m_f is the mass of the final state fermion, and $\beta \equiv \sqrt{1 - (4m_f^2/s)}$. $Q_{e_L f_R}$ etc. are given by

$$\begin{aligned}
Q_{e_L f_L} &\equiv \sum_i \frac{g_{V_i e}^L g_{V_i f}^L}{(s - m_{V_i}^2) + im_{V_i} \Gamma_{V_i}}, & Q_{e_L f_R} &\equiv \sum_i \frac{g_{V_i e}^L g_{V_i f}^R}{(s - m_{V_i}^2) + im_{V_i} \Gamma_{V_i}}, \\
Q_{e_R f_L} &\equiv \sum_i \frac{g_{V_i e}^R g_{V_i f}^L}{(s - m_{V_i}^2) + im_{V_i} \Gamma_{V_i}}, & Q_{e_R f_R} &\equiv \sum_i \frac{g_{V_i e}^R g_{V_i f}^R}{(s - m_{V_i}^2) + im_{V_i} \Gamma_{V_i}}, \tag{3.4}
\end{aligned}$$

where $g_{V_i f}^{L/R}$ are couplings of the left- and right-handed fermion f to the vector boson V_i , and m_{V_i} and Γ_{V_i} are the mass and total decay width of V_i . For $\sqrt{s} \gg m_f$ ($\beta \simeq 1$), the differential cross sections in Eq. (3.3) are approximated by

$$\begin{aligned}
\frac{d\sigma_{LR}^{f\bar{f}}}{d\cos\theta}(\cos\theta) &\simeq \frac{s}{32\pi} \left\{ (1 + \cos\theta)^2 |Q_{e_L f_L}|^2 + (1 - \cos\theta)^2 |Q_{e_L f_R}|^2 \right\}, \\
\frac{d\sigma_{RL}^{f\bar{f}}}{d\cos\theta}(\cos\theta) &\simeq \frac{s}{32\pi} \left\{ (1 + \cos\theta)^2 |Q_{e_R f_R}|^2 + (1 - \cos\theta)^2 |Q_{e_R f_L}|^2 \right\}. \tag{3.5}
\end{aligned}$$

We define $\sigma^{f\bar{f}}(P_{e^-}, P_{e^+}, [\cos\theta_1, \cos\theta_2])$ as the differential cross section integrated over the angle $\theta = [\theta_1, \theta_2]$:

$$\sigma^{f\bar{f}}(P_{e^-}, P_{e^+}, [\cos\theta_1, \cos\theta_2]) \equiv \int_{\cos\theta_1}^{\cos\theta_2} \frac{d\sigma^{f\bar{f}}}{d\cos\theta}(P_{e^-}, P_{e^+}, \cos\theta) d\cos\theta, \tag{3.6}$$

where $\frac{d\sigma^{f\bar{f}}}{d\cos\theta}(P_{e^-}, P_{e^+}, \cos\theta)$ is given in Eq. (3.1). The observed total cross section $\sigma_{\text{tot}}^{f\bar{f}}(P_{e^-}, P_{e^+})$ is given by

$$\sigma_{\text{tot}}^{f\bar{f}}(P_{e^-}, P_{e^+}) = \sigma^{f\bar{f}}(P_{e^-}, P_{e^+}, [-\cos\theta_{\text{max}}, +\cos\theta_{\text{max}}]), \tag{3.7}$$

where the available value of θ_{max} depends on each experiment. By using the cross sections for $e_L^- e_R^+ \rightarrow f\bar{f}$ and $e_R^- e_L^+ \rightarrow f\bar{f}$, the cross section $\sigma_{\text{tot}}^{f\bar{f}}(P_{e^-}, P_{e^+})$ can be written by

$$\sigma_{\text{tot}}^{f\bar{f}}(P_{e^-}, P_{e^+}) = (1 - P_{e^-} P_{e^+}) \cdot \frac{1}{4} \left\{ (1 - P_{\text{eff}}) \sigma_{LR}^{f\bar{f}} + (1 + P_{\text{eff}}) \sigma_{RL}^{f\bar{f}} \right\}. \tag{3.8}$$

$\sigma_{LR}^{f\bar{f}}$ and $\sigma_{RL}^{f\bar{f}}$ are given by

$$\sigma_{LR}^{f\bar{f}} = \int_{-\cos\theta_{\text{max}}}^{+\cos\theta_{\text{max}}} \frac{d\sigma_{LR}^{f\bar{f}}}{d\cos\theta}(\cos\theta) d\cos\theta,$$

$$\sigma_{RL}^{f\bar{f}} = \int_{-\cos\theta_{\max}}^{+\cos\theta_{\max}} \frac{d\sigma_{RL}^{f\bar{f}}}{d\cos\theta}(\cos\theta) d\cos\theta. \quad (3.9)$$

For $\cos\theta_{\max} = 1$

$$\begin{aligned} \sigma_{LR}^{f\bar{f}} &= \frac{\beta s}{32\pi} \left\{ \left[2 + \frac{2}{3}\beta^2 \right] \{ |Q_{e_L f_L}|^2 + |Q_{e_L f_R}|^2 \} + 16 \frac{m_f^2}{s} \text{Re}[Q_{e_L f_L} Q_{e_L f_R}^*] \right\}, \\ \sigma_{RL}^{f\bar{f}} &= \frac{\beta s}{32\pi} \left\{ \left[2 + \frac{2}{3}\beta^2 \right] \{ |Q_{e_R f_R}|^2 + |Q_{e_R f_L}|^2 \} + 16 \frac{m_f^2}{s} \text{Re}[Q_{e_R f_L} Q_{e_R f_R}^*] \right\}. \end{aligned} \quad (3.10)$$

Further, for $\sqrt{s} \gg m_f$

$$\begin{aligned} \sigma_{LR}^{f\bar{f}} &\simeq \frac{s}{12\pi} (|Q_{e_L f_L}|^2 + |Q_{e_L f_R}|^2), \\ \sigma_{RL}^{f\bar{f}} &\simeq \frac{s}{12\pi} (|Q_{e_R f_R}|^2 + |Q_{e_R f_L}|^2). \end{aligned} \quad (3.11)$$

The statistical error of the cross section $\Delta\sigma^{f\bar{f}}$ is given by

$$\begin{aligned} \Delta\sigma^{f\bar{f}}(P_{e^-}, P_{e^+}, [\cos\theta_1, \cos\theta_2]) &= \frac{\sigma^{f\bar{f}}(P_{e^-}, P_{e^+}, [\cos\theta_1, \cos\theta_2])}{\sqrt{N^{f\bar{f}}}}, \\ N^{f\bar{f}} &= L_{\text{int}} \cdot \sigma^{f\bar{f}}(P_{e^-}, P_{e^+}, [\cos\theta_1, \cos\theta_2]), \end{aligned} \quad (3.12)$$

where L_{int} is integrated luminosity. The amount of the deviation from the SM in the differential cross section for $e^-e^+ \rightarrow f\bar{f}$ is characterized by

$$\Delta_{d\sigma}^{f\bar{f}}(P_{e^-}, P_{e^+}, \cos\theta) \equiv \frac{\frac{d\sigma_{\text{GHU}}^{f\bar{f}}}{d\cos\theta}(P_{e^-}, P_{e^+}, \cos\theta)}{\frac{d\sigma_{\text{SM}}^{f\bar{f}}}{d\cos\theta}(P_{e^-}, P_{e^+}, \cos\theta)} - 1. \quad (3.13)$$

Similarly, for the total cross section we introduce

$$\Delta_{\sigma}^{f\bar{f}}(P_{e^-}, P_{e^+}) \equiv \frac{\sigma_{\text{GHU}}^{f\bar{f}}(P_{e^-}, P_{e^+})}{\sigma_{\text{SM}}^{f\bar{f}}(P_{e^-}, P_{e^+})} - 1. \quad (3.14)$$

3.2 Forward-backward asymmetry

The forward-backward asymmetry $A_{FB}^{f\bar{f}}(P_{e^-}, P_{e^+})$ [60, 61] is given by

$$\begin{aligned} A_{FB}^{f\bar{f}}(P_{e^-}, P_{e^+}) &= \frac{\sigma_F^{f\bar{f}}(P_{e^-}, P_{e^+}) - \sigma_B^{f\bar{f}}(P_{e^-}, P_{e^+})}{\sigma_F^{f\bar{f}}(P_{e^-}, P_{e^+}) + \sigma_B^{f\bar{f}}(P_{e^-}, P_{e^+})}, \\ \sigma_F^{f\bar{f}}(P_{e^-}, P_{e^+}) &= \sigma^{f\bar{f}}(P_{e^-}, P_{e^+}, [0, +\cos\theta_{\max}]), \\ \sigma_B^{f\bar{f}}(P_{e^-}, P_{e^+}) &= \sigma^{f\bar{f}}(P_{e^-}, P_{e^+}, [-\cos\theta_{\max}, 0]), \end{aligned} \quad (3.15)$$

where the available value of θ_{\max} depends on each experiment. For $\sqrt{s} \gg m_f$ and $\cos\theta_{\max} = 1$

$$A_{FB}^{f\bar{f}}(P_{e^-}, P_{e^+}) \simeq \frac{3B_1 - B_2}{4B_1 + B_2},$$

$$\begin{aligned}
B_1 &= (1 + P_{\text{eff}})|Q_{e_R f_R}|^2 + (1 - P_{\text{eff}})|Q_{e_L f_L}|^2 , \\
B_2 &= (1 + P_{\text{eff}})|Q_{e_R f_L}|^2 + (1 - P_{\text{eff}})|Q_{e_L f_R}|^2 ,
\end{aligned} \tag{3.16}$$

where P_{eff} is given in Eq. (3.2).

The statistical error of the forward-backward asymmetry $\Delta A_{FB}^{f\bar{f}}$ is given by

$$\begin{aligned}
\Delta A_{FB}^{f\bar{f}} &= 2 \frac{\sqrt{n_1 n_2} (\sqrt{n_1} + \sqrt{n_2})}{(n_1 + n_2)^2} \\
&= \frac{2\sqrt{n_1 n_2}}{(n_1 + n_2) (\sqrt{n_1} - \sqrt{n_2})} A_{FB}^{f\bar{f}} , \\
(n_1, n_2) &= (N_F^{f\bar{f}}, N_B^{f\bar{f}}) ,
\end{aligned} \tag{3.17}$$

where $N_{F/B}^{f\bar{f}} = L_{\text{int}} \cdot \sigma_{F/B}^{f\bar{f}}(P_{e^-}, P_{e^+})$ is the number of events. The amount of the deviation from the SM is characterized by

$$\Delta_{A_{FB}}^{f\bar{f}} \equiv \frac{A_{FB, \text{GHU}}^{f\bar{f}}}{A_{FB, \text{SM}}^{f\bar{f}}} - 1 . \tag{3.18}$$

3.3 Left-right asymmetry

The left-right asymmetry [34, 60, 61] is given by

$$A_{LR}^{f\bar{f}}(\cos \theta) = \frac{\sigma_{LR}^{f\bar{f}}(\cos \theta) - \sigma_{RL}^{f\bar{f}}(\cos \theta)}{\sigma_{LR}^{f\bar{f}}(\cos \theta) + \sigma_{RL}^{f\bar{f}}(\cos \theta)} , \tag{3.19}$$

where $\sigma_{LR}^{f\bar{f}}(\cos \theta)$ and $\sigma_{RL}^{f\bar{f}}(\cos \theta)$ stand for $\frac{d\sigma_{LR}^{f\bar{f}}}{d\cos \theta}(\cos \theta)$ and $\frac{d\sigma_{RL}^{f\bar{f}}}{d\cos \theta}(\cos \theta)$ in Eq. (3.3), respectively. For $\sqrt{s} \gg m_f$,

$$A_{LR}^{f\bar{f}}(\cos \theta) \simeq \frac{(1 + \cos \theta)^2 (|Q_{e_L f_L}|^2 - |Q_{e_R f_R}|^2) + (1 - \cos \theta)^2 (|Q_{e_L f_R}|^2 - |Q_{e_R f_L}|^2)}{(1 + \cos \theta)^2 (|Q_{e_L f_L}|^2 + |Q_{e_R f_R}|^2) + (1 - \cos \theta)^2 (|Q_{e_L f_R}|^2 + |Q_{e_R f_L}|^2)} . \tag{3.20}$$

The observable left-right asymmetry is given by

$$A_{LR}^{f\bar{f}}(P_{e^-}, P_{e^+}, \cos \theta) = \frac{\sigma^{f\bar{f}}(P_{e^-}, P_{e^+}, \cos \theta) - \sigma^{f\bar{f}}(-P_{e^-}, -P_{e^+}, \cos \theta)}{\sigma^{f\bar{f}}(P_{e^-}, P_{e^+}, \cos \theta) + \sigma^{f\bar{f}}(-P_{e^-}, -P_{e^+}, \cos \theta)} \tag{3.21}$$

for $P_{e^-} < 0$ and $|P_{e^-}| > |P_{e^+}|$, where $\sigma^{f\bar{f}}(P_{e^-}, P_{e^+}, \cos \theta)$ and $\sigma^{f\bar{f}}(-P_{e^-}, -P_{e^+}, \cos \theta)$ stand for $\frac{d\sigma^{f\bar{f}}}{d\cos \theta}(P_{e^-}, P_{e^+}, \cos \theta)$ and $\frac{d\sigma^{f\bar{f}}}{d\cos \theta}(-P_{e^-}, -P_{e^+}, \cos \theta)$ in Eq. (3.1), respectively. (3.21) is related to (3.19) by

$$A_{LR}^{f\bar{f}}(\cos \theta) = \frac{1}{P_{\text{eff}}} A_{LR}^{f\bar{f}}(P_{e^-}, P_{e^+}, \cos \theta) . \tag{3.22}$$

The integrated left-right asymmetry $A_{LR}^{f\bar{f}}$ [60, 61] is given by

$$A_{LR}^{f\bar{f}} = \frac{\sigma_{LR}^{f\bar{f}} - \sigma_{RL}^{f\bar{f}}}{\sigma_{LR}^{f\bar{f}} + \sigma_{RL}^{f\bar{f}}} . \quad (3.23)$$

In terms of $Q_{e_X f_Y}(X, Y = L, R)$ in Eq. (3.4), $A_{LR}^{f\bar{f}}$ is expressed as

$$\begin{aligned} A_{LR}^{f\bar{f}} &= \frac{C_-}{C_+} , \\ C_{\pm} &= \left(1 + \frac{1}{3}\beta^2\right) \left\{ [|Q_{e_L f_L}|^2 + |Q_{e_L f_R}|^2] \pm [|Q_{e_R f_R}|^2 + |Q_{e_R f_L}|^2] \right\} \\ &\quad + 8 \frac{m_f^2}{s} \left\{ \text{Re}(Q_{e_L f_L} Q_{e_L f_R}^*) \pm \text{Re}(Q_{e_R f_R} Q_{e_R f_L}^*) \right\} . \end{aligned} \quad (3.24)$$

For $\sqrt{s} \gg m_f$,

$$A_{LR}^{f\bar{f}} \simeq \frac{[|Q_{e_L f_L}|^2 + |Q_{e_L f_R}|^2] - [|Q_{e_R f_R}|^2 + |Q_{e_R f_L}|^2]}{[|Q_{e_L f_L}|^2 + |Q_{e_L f_R}|^2] + [|Q_{e_R f_R}|^2 + |Q_{e_R f_L}|^2]} . \quad (3.25)$$

The observable left-right asymmetry is given by

$$A_{LR}^{f\bar{f}}(P_{e^-}, P_{e^+}) = \frac{\sigma^{f\bar{f}}(P_{e^-}, P_{e^+}) - \sigma^{f\bar{f}}(-P_{e^-}, -P_{e^+})}{\sigma^{f\bar{f}}(P_{e^-}, P_{e^+}) + \sigma^{f\bar{f}}(-P_{e^-}, -P_{e^+})} \quad (3.26)$$

for $P_{e^-} < 0$ and $|P_{e^-}| > |P_{e^+}|$. It is related to (3.23) by

$$A_{LR}^{f\bar{f}} = \frac{1}{P_{\text{eff}}} A_{LR}^{f\bar{f}}(P_{e^-}, P_{e^+}) . \quad (3.27)$$

The statistical error of the left-right asymmetry $\Delta A_{LR}^{f\bar{f}}$ is given by

$$\begin{aligned} \Delta A_{LR}^{f\bar{f}} &= 2 \frac{\sqrt{N_{LR}^{f\bar{f}} N_{RL}^{f\bar{f}}} \left(\sqrt{N_{LR}^{f\bar{f}}} + \sqrt{N_{RL}^{f\bar{f}}} \right)}{(N_{LR}^{f\bar{f}} + N_{RL}^{f\bar{f}})^2} \\ &= \frac{2 \sqrt{N_{LR}^{f\bar{f}} N_{RL}^{f\bar{f}}}}{(N_{LR}^{f\bar{f}} + N_{RL}^{f\bar{f}}) \left(\sqrt{N_{LR}^{f\bar{f}}} - \sqrt{N_{RL}^{f\bar{f}}} \right)} A_{LR}^{f\bar{f}} , \end{aligned} \quad (3.28)$$

where $N_{LR}^{f\bar{f}} = L_{\text{int}} \sigma_{LR}^{f\bar{f}}$ and $N_{RL}^{f\bar{f}} = L_{\text{int}} \sigma_{RL}^{f\bar{f}}$ are the numbers of the events. The amount of the deviation from the SM in (3.22) and (3.23) is characterized by

$$\begin{aligned} \Delta_{A_{LR}}^{f\bar{f}}(\cos \theta) &\equiv \frac{A_{LR, \text{GHU}}^{f\bar{f}}(\cos \theta)}{A_{LR, \text{SM}}^{f\bar{f}}(\cos \theta)} - 1 , \\ \Delta_{A_{LR}}^{f\bar{f}} &\equiv \frac{A_{LR, \text{GHU}}^{f\bar{f}}}{A_{LR, \text{SM}}^{f\bar{f}}} - 1 . \end{aligned} \quad (3.29)$$

3.4 Left-right forward-backward asymmetry

The left-right forward-backward asymmetry [61, 64–67] is given by

$$A_{LR,FB}^{f\bar{f}}(\cos\theta) = \frac{\left[\sigma_{LR}^{f\bar{f}}(\cos\theta) - \sigma_{RL}^{f\bar{f}}(\cos\theta)\right] - \left[\sigma_{LR}^{f\bar{f}}(-\cos\theta) - \sigma_{RL}^{f\bar{f}}(-\cos\theta)\right]}{\left[\sigma_{LR}^{f\bar{f}}(\cos\theta) + \sigma_{RL}^{f\bar{f}}(\cos\theta)\right] + \left[\sigma_{LR}^{f\bar{f}}(-\cos\theta) + \sigma_{RL}^{f\bar{f}}(-\cos\theta)\right]} . \quad (3.30)$$

In terms of $Q_{e_X f_Y}(X, Y = L, R)$ in Eq. (3.4), $A_{LR,FB}^{f\bar{f}}$ is expressed as

$$\begin{aligned} A_{LR,FB}^{f\bar{f}}(\cos\theta) &= \frac{2\beta \cos\theta D_-}{(1 + \beta^2 \cos^2\theta)D_+ + 8(m_f^2/s) [\text{Re}(Q_{e_L f_L} Q_{e_L f_R}^*) + \text{Re}(Q_{e_R f_R} Q_{e_R f_L}^*)]} , \\ D_{\pm} &= (|Q_{e_L f_L}|^2 + |Q_{e_R f_L}|^2) \pm (|Q_{e_L f_R}|^2 + |Q_{e_R f_R}|^2) . \end{aligned} \quad (3.31)$$

For $\sqrt{s} \gg m_f$,

$$A_{LR,FB}^{f\bar{f}}(\cos\theta) \simeq \frac{2 \cos\theta}{1 + \cos^2\theta} \frac{D_-}{D_+} \quad (3.32)$$

The observable left-right forward-backward asymmetry is given by

$$\begin{aligned} A_{LR,FB}^{f\bar{f}}(P_{e^-}, P_{e^+}, \cos\theta) &= \frac{E_-}{E_+} , \\ E_{\pm} &= [\sigma^{f\bar{f}}(P_{e^-}, P_{e^+}, \cos\theta) + \sigma^{f\bar{f}}(-P_{e^-}, -P_{e^+}, -\cos\theta)] \\ &\quad \pm [\sigma^{f\bar{f}}(-P_{e^-}, -P_{e^+}, \cos\theta) + \sigma^{f\bar{f}}(P_{e^-}, P_{e^+}, -\cos\theta)] \end{aligned} \quad (3.33)$$

for $P_{e^-} < 0$ and $|P_{e^-}| > |P_{e^+}|$. The relation between $A_{LR,FB}^{f\bar{f}}(\cos\theta)$ in Eq. (3.30) and $A_{LR,FB}^{f\bar{f}}(P_{e^-}, P_{e^+}, \cos\theta)$ in Eq. (3.33) is given by

$$A_{LR,FB}^{f\bar{f}}(\cos\theta) = \frac{1}{P_{\text{eff}}} A_{LR,FB}^{f\bar{f}}(P_{e^-}, P_{e^+}, \cos\theta) . \quad (3.34)$$

The statistical error of the left-right forward-backward asymmetry $\Delta A_{LR,FB}$ is given by

$$\begin{aligned} \Delta A_{LR,FB} &= 2 \frac{(n_3 + n_2) (\sqrt{n_1} + \sqrt{n_4}) + (n_1 + n_4) (\sqrt{n_3} + \sqrt{n_2})}{(n_1 + n_3 + n_2 + n_4)^2} \\ &= 2 \frac{(n_3 + n_2) (\sqrt{n_1} + \sqrt{n_4}) + (n_1 + n_4) (\sqrt{n_3} + \sqrt{n_2})}{(n_1 + n_4)^2 - (n_3 + n_2)^2} A_{LR,FB} , \\ (n_1, n_2, n_3, n_4) &= (N_{LRF}^{f\bar{f}}, N_{RLF}^{f\bar{f}}, N_{LRB}^{f\bar{f}}, N_{RLB}^{f\bar{f}}) , \end{aligned} \quad (3.35)$$

where $N_{XF}^{f\bar{f}} = L_{\text{int}} \cdot \sigma_X^{f\bar{f}}([\cos\theta_1, \cos\theta_2])$ and $N_{XB}^{f\bar{f}} = L_{\text{int}} \cdot \sigma_X^{f\bar{f}}([-\cos\theta_2, -\cos\theta_1])$ ($X = LR, RL$; $0 < \cos\theta_1 < \cos\theta_2$) are the numbers of the events. The amount of the deviation in $A_{LR,FB}$ from the SM is characterized by

$$\Delta_{A_{LR,FB}}^{f\bar{f}}(\cos\theta) \equiv \frac{A_{LR,FB,\text{GHU}}^{f\bar{f}}(\cos\theta)}{A_{LR,FB,\text{SM}}^{f\bar{f}}(\cos\theta)} - 1 . \quad (3.36)$$

4 Fermion pair production via Z' mediation

In this section we calculate various observables of the s -channel scattering process of $e^-e^+ \rightarrow f\bar{f}$ mediated by neutral vector bosons V in the GHU, where $V = \gamma, Z, Z^{(n)}, Z_R^{(n)}, \gamma^{(n)}$ ($n \geq 1$), and $f\bar{f} = \mu^-\mu^+, c\bar{c}, b\bar{b}, t\bar{t}$.

4.1 Parameter sets

Parameters of the model are determined in the steps described in Refs. [13–15].

- (i) We pick the values of θ_H and $m_{KK} = \pi k(z_L - 1)^{-1}$.
- (ii) k is determined in order for the Z boson mass m_Z to be reproduced, which fixes the warped factor z_L as well.
- (iii) The bare Weinberg angle θ_W^0 in Eq. (2.8) with given θ_H is not known beforehand. It is determined self-consistently to fit the observed forward-backward asymmetry $A_{FB}(e^-e^+ \rightarrow \mu^-\mu^+) = 0.0169 \pm 0.0013$ at $\sqrt{s} = m_Z$ [80, 81], after evaluating the lepton gauge couplings with the procedure described below. We have checked that self-consistent value of θ_W^0 is found after a couple of iterations of this process. For instance, for $\theta_H = 0.10$ and $m_{KK} = 13$ TeV, $\sin \theta_W^0 = 0.2305$ yields $A_{FB}(e^-e^+ \rightarrow \mu^-\mu^+) = 0.01693$ at $\sqrt{s} = m_Z$. If one chooses $\sin \theta_W^0 = 0.2313$ (0.2298) instead, then one finds $A_{FB}(e^-e^+ \rightarrow \mu^-\mu^+) = 0.01562$ (0.01821). It has been shown in [11, 12] that $\sin \theta_W^0 = 0.2305$ yields W and Z coupling constants of quarks and leptons which are nearly the same as those in the SM with $\sin^2 \theta_W = 0.2312$. In our analysis, we will use the values of $\sin \theta_W^0$ for each set of θ_H and m_{KK} that reproduce the central value of $A_{FB}(e^-e^+ \rightarrow \mu^-\mu^+)$.
- (iv) With given $\sin \theta_W^0$, wave functions of gauge bosons are fixed.
- (v) The bulk mass parameters of $\Psi_{(3,4)}^\alpha$ and $\Psi_{(1,4)}^\alpha$ are fixed from the masses of up-type quarks and charged leptons.
- (vi) The bulk mass parameters of $\Psi_{(3,1)}^{\pm\alpha}$ and brane interaction coefficients in the down-quark sector are determined so as to reproduce the masses of down-type quarks. Similarly the Majorana mass terms and brane interactions in the neutrino sector are determined so as to reproduce neutrino masses. We use the masses of quarks and leptons given by $m_u = 20$ MeV, $m_c = 619$ MeV, $m_t = 172.9$ GeV, $m_d = 2.9$ MeV, $m_s = 55$ MeV, $m_b = 2.89$ GeV, $m_e = 0.486$ MeV, $m_\mu = 102.7$ MeV, $m_\tau = 1.746$ GeV, $m_{\nu_e} = m_{\nu_\mu} = m_{\nu_\tau} = 10^{-12}$ GeV. As discussed in Ref. [13], left-handed and right-handed up- and down-type quarks (u, d, u', d') , (c, s, c', s') , (t, b, t', b') belong to the same multiplet $\Psi_{(3,4)}^\alpha$ shown in Table 2 in each generation so that the up- and down-type quarks have a degenerate mass in each generation in the absence of mixing among $(d, d'), (s, s'), (b, b')$ and $D_d^\pm, D_s^\pm, D_b^\pm$, respectively. The mixing resolves the degeneracy between up- and down-type quarks in

each generation, but always makes the down-type quark lighter than the up-type quark. For this reason we adopt the value $m_u > m_d$ at the moment. It is left as a future task to explain the observed m_u in the GUT inspired GHU.

With these parameters fixed, wave functions of quarks and leptons are determined. In the present paper we mostly ignore the flavor mixing in the quark and lepton gauge couplings [14, 82–88]. It has been shown that the Cabibbo-Kobayashi-Maskawa (CKM) mixing matrix can be incorporated in GHU with naturally suppressed FCNCs (flavor changing neutral currents) [14]. FCNC couplings are suppressed by a factor of $O(10^{-6})$. There arise flavor changing couplings of Z' bosons in the down-type quark sector. For $\theta_H = 0.1$ and $m_{KK} = 13 \text{ TeV}$, the $Z^{(1)}$ couplings in the down-type quark sector, for instance, are given by

$$\begin{aligned} g_{Z^{(1)d}}^L &= \begin{pmatrix} -2.6792 & -0.0215 & -0.0001 \\ -0.0215 & -2.5907 & -0.0018 \\ -0.0001 & -0.0018 & -2.1284 \end{pmatrix} g_w, \\ g_{Z^{(1)d}}^R &= \begin{pmatrix} 0.1907 & -0.0420 & 0.0144 \\ -0.0420 & 0.0301 & -0.0436 \\ 0.0144 & -0.0436 & 0.2786 \end{pmatrix} g_w \end{aligned} \quad (4.1)$$

with typical brane interactions yielding the CKM matrix approximately. Flavor changing Z' couplings in the left-handed components are very small compared to diagonal ones. Flavor changing Z' couplings in the right-handed components are slightly bigger, but their magnitude is small. In the processes $e^-e^+ \rightarrow f\bar{f}$, the effect of flavor changing Z' couplings remains very small for $\sqrt{s} < 3 \text{ TeV}$. In the following analysis we shall safely ignore these flavor changing Z' couplings in the down-type quark sector.

With the parameter set given, the Z' coupling constants to the SM fermions, etc. are determined. To evaluate the cross section and other quantities in the processes $e^-e^+ \rightarrow f\bar{f}$, we need to know the four-dimensional Z' couplings of quarks and leptons. They are obtained from the five-dimensional gauge interaction terms by inserting wave functions of gauge bosons and quarks or leptons and integrating over the fifth-dimensional coordinate [11, 12, 16]. Decay widths of Z' bosons are calculated by using the formulas in Appendix A with masses and various couplings of Z' bosons. (For the total decay widths of Z' s, we take into account the two body decays at tree level approximation.) The masses and widths of γ , Z boson, and the first neutral KK vector bosons $Z^{(1)}$, $Z_R^{(1)}$, $\gamma^{(1)}$ are listed in Table 3. The coupling constants of Z boson and the first neutral KK vector bosons $Z^{(1)}$, $Z_R^{(1)}$, $\gamma^{(1)}$ to quarks and leptons are listed in Tables 4, 5, 6, 7, 8. In Table 9, masses of neutral higher KK vector bosons $Z^{(2k-1)}$, $Z^{(2k)}$, $Z_R^{(k)}$, $\gamma^{(k)}$ ($k = 1, 2, \dots, 10$) and their couplings constants to left- and right-handed electrons are summarized. We note that possible values of z_L is

restricted with given θ_H . It has been shown in Ref. [15] that for $\theta_H = 0.10$ the top quark mass can be reproduced only if $z_L \geq 10^{8.1}$ and dynamical electroweak symmetry breaking is achieved only if $z_L \leq 10^{15.5}$, the values of which correspond to $m_{KK} \simeq [11, 15]$ TeV.

Name	θ_H [rad.]	m_{KK} [TeV]	z_L	k [GeV]	$m_{\gamma^{(1)}}$ [TeV]	$\Gamma_{\gamma^{(1)}}$ [TeV]	$m_{Z^{(1)}}$ [TeV]	$\Gamma_{Z^{(1)}}$ [TeV]	$m_{Z_R^{(1)}}$ [TeV]	$\Gamma_{Z_R^{(1)}}$ [TeV]	Table
B ^L	0.10	11.00	1.980×10^8	6.933×10^{11}	8.715	2.080	8.713	4.773	8.420	0.603	5
B	0.10	13.00	3.865×10^{11}	1.599×10^{15}	10.20	3.252	10.20	7.840	9.951	0.816	4
B ^H	0.10	15.00	2.667×10^{15}	1.273×10^{19}	11.69	4.885	11.69	11.82	11.48	1.253	6

Name	θ_H [rad.]	m_{KK} [TeV]	z_L	k [GeV]	$m_{\gamma^{(1)}}$ [TeV]	$\Gamma_{\gamma^{(1)}}$ [TeV]	$m_{Z^{(1)}}$ [TeV]	$\Gamma_{Z^{(1)}}$ [TeV]	$m_{Z_R^{(1)}}$ [TeV]	$\Gamma_{Z_R^{(1)}}$ [TeV]	Table
B ⁺	0.11	13.00	1.021×10^{14}	4.223×10^{17}	10.15	3.836	10.15	9.374	9.951	0.924	7
B	0.10	13.00	3.865×10^{11}	1.599×10^{15}	10.20	3.252	10.20	7.840	9.951	0.816	4
B ⁻	0.09	13.00	2.470×10^9	1.022×10^{13}	10.26	2.723	10.26	6.413	9.951	0.732	8

Table 3: Masses and widths of Z' bosons ($Z^{(1)}$, $\gamma^{(1)}$, and $Z_R^{(1)}$) are listed for $\theta_H = 0.10$ and three $m_{KK} = 11, 13, 15$ TeV values in the upper table, and $m_{KK} = 13$ TeV and three $\theta_H = 0.11, 0.10, 0.09$ values in the lower table. $m_Z = 91.1876$ GeV and $\Gamma_Z = 2.4952$ GeV [81]. The column “Name” denotes each parameter set and the column “Table” indicate the table summarizing coupling constants in each set.

It is seen from Table 3 that for the same KK mass scale m_{KK} and different θ_H , the masses of the first neutral KK vector bosons $Z^{(1)}$, $Z_R^{(1)}$, $\gamma^{(1)}$ are almost the same, while the decay widths of $Z^{(1)}$, $Z_R^{(1)}$, and $\gamma^{(1)}$ become smaller for smaller θ_H . For the same θ_H , the masses and decay widths of the first neutral KK vector bosons $Z^{(1)}$, $Z_R^{(1)}$, and $\gamma^{(1)}$ become larger for larger m_{KK} . The total decay widths satisfy the relation $\Gamma_{Z^{(1)}} > \Gamma_{\gamma^{(1)}} \gg \Gamma_{Z_R^{(1)}}$.

From Tables 4, 5, 6, 7, 8, we find that the coupling constants of the first neutral KK vector bosons $Z^{(1)}$, $Z_R^{(1)}$, $\gamma^{(1)}$ to quarks and leptons are larger than those of the right-handed fermions except for $Z_R^{(1)}$ couplings to the top and bottom quarks.

In Table 9, the masses of neutral higher KK vector bosons $Z^{(2k-1)}$, $Z^{(2k)}$, $Z_R^{(k)}$, and $\gamma^{(k)}$ ($k = 1, 2, \dots, 10$) almost linearly increase as k . For instance, $m_{Z^{(n)}}/m_{KK} = 0.784, 1.220, 1.777, 2.233, 2.775, 3.238, \dots$ for $n = 1, 2, 3, \dots$. The couplings constants of them to left- and right-handed electrons is decreasing when k is increasing. In Figure 1, total cross section $\sigma(e^-e^+ \rightarrow \mu^-\mu^+)$ with and without the contribution from the second KK modes for $\theta_H = 0.10$ and $m_{KK} = 13$ TeV (B) is shown. The coupling constants of the 1st KK bosons to the SM fermions are listed in Table 4. The masses and widths of the second KK bosons are given by $(m_{Z^{(2)}}, \Gamma_{Z^{(2)}}) = (15.86, 0.876)$, $(m_{Z^{(3)}}, \Gamma_{Z^{(3)}}) = (23.10, 1.498)$, $(m_{Z_R^{(2)}}, \Gamma_{Z_R^{(2)}}) = (22.84, 0.160)$, $(m_{\gamma^{(2)}}, \Gamma_{\gamma^{(2)}}) = (23.10, 0.645)$ in units of TeV, where the decay widths include only the final states of the SM fermions and bosons. The coupling constants of the second KK bosons to e are found in Table 9. The coupling constants

f	g_{Zf}^L	g_{Zf}^R	$g_{Z^{(1)}f}^L$	$g_{Z^{(1)}f}^R$	$g_{Z_R^{(1)}f}^L$	$g_{Z_R^{(1)}f}^R$	$g_{\gamma^{(1)}f}^L$	$g_{\gamma^{(1)}f}^R$
ν_e	0.5687	0	3.2774	0	-1.0322	0	0	0
ν_μ	0.5687	0	3.1207	0	-0.9852	0	0	0
ν_τ	0.5687	0	3.0165	0	-0.9539	0	0	0
e	-0.3058	0.2629	-1.7621	-0.0584	-1.0444	0	-2.7587	0.1071
μ	-0.3058	0.2629	-1.6778	-0.0584	-0.9969	0	-2.6268	0.1071
τ	-0.3058	0.2629	-1.6218	-0.0584	-0.9652	0.0001	-2.5391	0.1070
u	0.3934	-0.1753	2.1951	0.0390	0.3415	0	1.7807	-0.0714
c	0.3934	-0.1753	2.1147	0.0389	0.3296	0	1.7154	-0.0714
t	0.3938	-0.1749	1.7406	-0.3269	0.2740	-0.7395	1.4121	0.6017
d	-0.4811	0.0876	-2.6842	0.1162	0.3297	-0.1801	-0.8904	-0.2113
s	-0.4811	0.0876	-2.5858	0.1460	0.3182	-0.2197	-0.8577	-0.2657
b	-0.4811	0.0876	-2.1284	0.2900	0.2646	-0.4096	-0.7059	-0.5279

Table 4: Coupling constants of neutral vector bosons, Z' bosons, to fermions in units of $g_w = e/\sin\theta_W^0$ are listed for $\theta_H = 0.10$ and $m_{KK} = 13.00$ TeV (B) in Table 3, where $\sin^2\theta_W^0 = 0.2306$. Their corresponding Z boson coupling constants in the SM are $(g_{Z\nu}^L, g_{Z\nu}^R) = (0.5703, 0)$, $(g_{Ze}^L, g_{Ze}^R) = (-0.3065, 0.2638)$, $(g_{Zu}^L, g_{Zu}^R) = (0.3944, -0.1748)$, $(g_{Zd}^L, g_{Zd}^R) = (-0.4823, 0.0879)$. Their corresponding γ boson coupling constants are the same as those in the SM. When the value is less than 10^{-4} , we write 0.

of the second KK bosons to μ are $(g_{Z^{(2)}\mu}^L, g_{Z^{(2)}\mu}^R) = (-0.0057, -0.0040)$, $(g_{Z^{(3)}\mu}^L, g_{Z^{(3)}\mu}^R) = (-0.5301, +0.0403)$, $(g_{Z_R^{(2)}\mu}^L, g_{Z_R^{(2)}\mu}^R) = (-0.3198, 0)$, $(g_{\gamma^{(2)}\mu}^L, g_{\gamma^{(2)}\mu}^R) = (-0.8299, -0.0739)$. The contribution for the low-energy observables from each higher KK vector boson $Z^{(k)}$, $Z_R^{(k)}$, $\gamma^{(k)}$ ($k \geq 2$) is sub-dominant. In the following, we consider contributions for the low-energy observables only from the first KK bosons $Z^{(1)}$, $Z_R^{(1)}$, and $\gamma^{(1)}$.

4.2 Cross section

Total cross sections $\sigma^{f\bar{f}}$ for $e^-e^+ \rightarrow f\bar{f}$ ($f\bar{f} = \mu^-\mu^+, c\bar{c}, b\bar{b}, t\bar{t}$) are plotted with various polarization $(P_{e-}, P_{e+}) = (0, 0), (-0.8, +0.3), (+0.8, -0.3)$ in Figures 2 and 3. On the left side in Figure 2 the \sqrt{s} dependence is shown. On the right side the amount of the deviation from the SM, $\Delta_\sigma^{f\bar{f}}$ defined in Eq. (3.14), is shown. One can see large deviation for $(P_{e-}, P_{e+}) = (-0.8, +0.3)$ in the B-model. It is due to the fact that the coupling constants of the left-handed electron and μ to Z' bosons are much larger than those of the right-handed ones as seen in Table 4. Distinct signals of GHU can be clearly observed in the e^-e^+ collision experiments at $\sqrt{s} = 250$ GeV even with 250 fb^{-1} data by examining polarization dependence. $\sigma^{f\bar{f}}(s)$ in wider range of \sqrt{s} is displayed in Figure 3.

Cross sections are determined in terms of $Q_{e_X f_Y}$ ($X, Y = L, R$) in (3.4). In Figure 4

f	g_{Zf}^L	g_{Zf}^R	$g_{Z^{(1)}f}^L$	$g_{Z^{(1)}f}^R$	$g_{Z_R^{(1)}f}^L$	$g_{Z_R^{(1)}f}^R$	$g_{\gamma^{(1)}f}^L$	$g_{\gamma^{(1)}f}^R$
ν_e	0.5688	0	2.8639	0	-0.9037	0	0	0
ν_μ	0.5687	0	2.7053	0	-0.8569	0	0	0
ν_τ	0.5687	0	2.5929	0	-0.8237	0	0	0
e	-0.3058	0.2629	-1.5398	-0.0695	-0.9143	0	-2.4107	0.1274
μ	-0.3058	0.2629	-1.4545	-0.0695	-0.8670	0	-2.2772	0.1274
τ	-0.3058	0.2629	-1.3940	-0.0694	-0.8334	0	-2.1824	0.1272
u	0.3934	-0.1753	1.9092	0.0463	0.2979	0	1.5487	-0.0849
c	0.3934	-0.1753	1.8243	0.0463	0.2855	0	1.4799	-0.0849
t	0.3940	-0.1747	1.2374	-0.4429	0.1993	-0.9777	1.0041	0.8145
d	-0.4811	0.0876	-2.3345	0.1280	0.2876	-0.1989	-0.7744	-0.2328
s	-0.4811	0.0876	-2.2308	0.1280	0.2756	-0.2394	-0.7399	-0.2892
b	-0.4811	0.0877	-1.5138	0.3256	0.1927	-0.4562	-0.5020	-0.5928

Table 5: Coupling constants of neutral vector bosons, Z' bosons, to fermions in units of $g_w = e/\sin\theta_W^0$ are listed for $\theta_H = 0.10$ and $m_{KK} = 11.00$ TeV (B^L) in Table 3, where $\sin^2\theta_W^0 = 0.2306$. Other information is the same as in Table 4.

\sqrt{s} -dependence of $s|Q_{e_X f_Y}|$ is displayed. In the SM, for $e^-e^+ \rightarrow \mu^-\mu^+$ for instance,

$$Q_{e_X \mu_Y}^{\text{SM}} = \frac{e^2}{s} + \frac{g_{Ze}^X g_{Z\mu}^Y g_w^2}{(s - m_Z^2) + im_Z \Gamma_Z},$$

$$|sQ_{e_X \mu_Y}^{\text{SM}}|^2 = e^4 + \frac{(g_{Ze}^X g_{Z\mu}^Y g_w^2)^2 s^2}{(s - m_Z^2)^2 + m_Z^2 \Gamma_Z^2} + \frac{2e^2 g_{Ze}^X g_{Z\mu}^Y g_w^2 s(s - m_Z^2)}{(s - m_Z^2)^2 + m_Z^2 \Gamma_Z^2}. \quad (4.2)$$

$s|Q_{e_X \mu_Y}|$ has peak at $\sqrt{s} = m_Z$ and $Q_{e_L \mu_R} = Q_{e_R \mu_L}$. $Q_{e_L \mu_L} = Q_{e_R \mu_R}$ becomes smaller below $\sqrt{s} = m_Z$ and $Q_{e_L \mu_R}$ and $Q_{e_R \mu_L}$ become smaller above $\sqrt{s} = m_Z$ as a result of the interference of the γ and Z amplitudes. We also note that $sQ_{e_X f_Y} \simeq e^2 + g_{Ze}^X g_{Zf}^Y g_w^2$ for $\sqrt{s} \gg m_Z$.

In GHU

$$Q_{e_X f_Y} = Q_{e_X f_Y}^{\text{SM}} + Q_{e_X f_Y}^{Z'},$$

$$Q_{e_X f_Y}^{Z'} \simeq \sum_{V=Z^{(1)}, \gamma^{(1)}, Z_R^{(1)}} \frac{g_{Ve}^X g_{Vf}^Y g_w^2}{(s - m_V^2) + im_V \Gamma_V}, \quad (4.3)$$

where we have retained contributions from first KK modes in $Q_{e_X f_Y}^{Z'}$. For $\sqrt{s} \lesssim 200$ GeV, $Q_{e_X f_Y} \sim Q_{e_X f_Y}^{\text{SM}}$ to good approximation. In Figure 4 the \sqrt{s} -dependence of $s|Q_{e_X f_Y}|$ is plotted. $Q_{e_X f_Y}$ has a peak around $\sqrt{s} \simeq m_{Z'} \simeq 10$ TeV. The dominant component is $Q_{e_L f_L}$, which develops significant deviation from the SM. $Q_{e_L f_L}$ has a dip around $\sqrt{s} \simeq 1.7$ TeV. For $f = b, t$, an additional dip is seen in the 2–5 TeV region for $Q_{e_L f_R}$.

We stress that due to the interference effects among γ , Z and Z' bosons, the GHU prediction for the total cross section shown in Figures 2 and 3 deviates from that in the

f	g_{Zf}^L	g_{Zf}^R	$g_{Z^{(1)}f}^L$	$g_{Z^{(1)}f}^R$	$g_{Z_R^{(1)}f}^L$	$g_{Z_R^{(1)}f}^R$	$g_{\gamma^{(1)}f}^L$	$g_{\gamma^{(1)}f}^R$
ν_e	0.5687	0	3.6903	0	-1.1603	0	0	0
ν_μ	0.5687	0	3.5400	0	-1.1147	0	0	0
ν_τ	0.5687	0	3.4442	0	-1.0857	0	0	0
e	-0.3057	0.2629	-1.9841	-0.0504	-1.1740	0	-3.1063	0.0924
μ	-0.3057	0.2629	-1.9033	-0.0504	-1.1279	0	-2.9780	0.0924
τ	-0.3057	0.2629	-1.8518	-0.0504	-1.0985	0	-2.8991	0.0923
u	0.3934	-0.1753	2.4831	0.0336	0.3855	0	2.0143	-0.0616
c	0.3934	-0.1753	2.4080	0.0336	0.3742	0	1.9534	-0.0616
t	0.3937	-0.1750	2.1069	-0.2768	0.3291	-0.6311	1.7092	0.5096
d	-0.4810	0.0876	-3.0363	0.1055	0.3721	-0.1632	-1.0072	-0.1919
s	-0.4810	0.0876	-2.9446	0.1337	0.3613	-0.2009	-0.9767	-0.2433
b	-0.4810	0.0876	-2.5762	0.1887	0.3178	-0.1691	-0.8545	-0.3440

Table 6: Coupling constants of neutral vector bosons, Z' bosons, to fermions in units of $g_w = e/\sin\theta_W^0$ are listed for $\theta_H = 0.10$ and $m_{KK} = 15.00$ TeV (B^H) in Table 3, where $\sin^2\theta_W^0 = 0.2306$. Other information is the same as in Table 4.

SM even well below the masses of Z' bosons. Also, from Figure 4, the behavior of the various components of the scattering amplitudes $Q_{e_X f_Y}$ is different so that by using the polarized electron-positron beams, one can investigate physics at 10 TeV region in more detail than with unpolarized beams.

Let us look at differential cross sections. In Figure 5, $d\sigma^{f\bar{f}}/d\cos\theta$ are shown for $f\bar{f} = \mu^-\mu^+, c\bar{c}, b\bar{b}$, at $\sqrt{s} = 250$ GeV and for $f\bar{f} = t\bar{t}$ at $\sqrt{s} = 500$ GeV. Differential cross sections in the forward region are larger than those of the backward region ($\cos\theta = [0, 1]$) regardless of the polarization. The deviation from the SM are seen in the forward region with less statistical errors. The differential cross sections of the 100% left- and right-handed polarized initial electron are given by the formulas in Eq. (3.5). In the SM the Z couplings are different for left-handed and right-handed fermions which leads to $Q_{e_L f_L} \neq Q_{e_L f_R}$ and $Q_{e_R f_R} \neq Q_{e_R f_L}$ and therefore forward-backward asymmetry.

In GHU coupling constants of the left-handed fermions to Z' bosons are, in most cases, much larger than those of the right-handed ones. The magnitude of the left-handed fermion couplings is rather large so that the amount of the deviation in $d\sigma^{f\bar{f}}/d\cos\theta$ from the SM becomes large for either left-handed polarized or unpolarized electron beams, whereas the deviation becomes small for right-handed electron beams. $\Delta_{d\sigma}^{f\bar{f}}(P_{e^-}, P_{e^+}, \cos\theta)$ in (3.13) is plotted in the right column of Figure 5. The deviation can be clearly seen in e^-e^+ collisions at $\sqrt{s} = 250$ GeV with 250 fb^{-1} data for $f\bar{f} = \mu^-\mu^+, c\bar{c}, b\bar{b}$ and at $\sqrt{s} = 500$ GeV with 500 fb^{-1} data for $f\bar{f} = t\bar{t}$.

f	g_{Zf}^L	g_{Zf}^R	$g_{Z^{(1)}f}^L$	$g_{Z^{(1)}f}^R$	$g_{Z_R^{(1)}f}^L$	$g_{Z_R^{(1)}f}^R$	$g_{\gamma^{(1)}f}^L$	$g_{\gamma^{(1)}f}^R$
ν_e	0.5684	0	3.5449	0	-1.1125	0	0	0
ν_μ	0.5684	0	3.3920	0	-1.0664	0	0	0
ν_τ	0.5684	0	3.2933	0	-1.0367	0	0	0
e	-0.3056	0.2628	-1.9057	-0.0529	-1.1284	0	-2.9829	0.0971
μ	-0.3056	0.2628	-1.8235	-0.0529	-1.0817	0	-2.8543	0.0971
τ	-0.3056	0.2628	-1.7705	-0.0529	-1.0515	0	-2.7712	0.0970
u	0.3932	-0.1752	2.3814	0.0353	0.3709	0	1.9313	-0.0647
c	0.3932	-0.1752	2.3044	0.0353	0.3594	0	1.8688	-0.0647
t	0.3935	-0.1748	1.9823	-0.2910	0.3111	-0.6640	1.6078	0.5369
d	-0.4808	0.0876	-2.9120	0.1091	0.3554	-0.1688	-0.9656	-0.1984
s	-0.4808	0.0876	-2.8179	0.1380	0.3444	-0.2071	-0.9344	-0.2509
b	-0.4807	0.0876	-2.4235	0.2760	0.2981	-0.3898	-0.8036	-0.5021

Table 7: Coupling constants of neutral vector bosons, Z' bosons, to fermions in units of $g_w = e/\sin\theta_W^0$ are listed for $\theta_H = 0.11$ and $m_{KK} = 13.00$ TeV (B^+) in Table 3, where $\sin^2\theta_W^0 = 0.2305$. Other information is the same as in Table 4.

4.3 Forward-backward asymmetry

The forward-backward asymmetry $A_{FB}^{f\bar{f}}$ is shown in Figure 6. From Eq. (3.15), $A_{FB}^{f\bar{f}}(P_{e^-}, P_{e^+})$ with $(P_{e^-}, P_{e^+}) = (0, 0), (-1, 0), (+1, 0)$ are given by

$$\begin{aligned}
A_{FB}^{f\bar{f}}(0, 0) &\simeq \frac{3 \{ |Q_{e_R f_R}|^2 + |Q_{e_L f_L}|^2 \} - \{ |Q_{e_R f_L}|^2 + |Q_{e_L f_R}|^2 \}}{4 \{ |Q_{e_R f_R}|^2 + |Q_{e_L f_L}|^2 \} + \{ |Q_{e_R f_L}|^2 + |Q_{e_L f_R}|^2 \}}, \\
A_{FB}^{f\bar{f}}(-1, 0) &\simeq \frac{3 |Q_{e_L f_L}|^2 - |Q_{e_L f_R}|^2}{4 |Q_{e_L f_L}|^2 + |Q_{e_L f_R}|^2}, \\
A_{FB}^{f\bar{f}}(1, 0) &\simeq \frac{3 |Q_{e_R f_R}|^2 - |Q_{e_R f_L}|^2}{4 |Q_{e_R f_R}|^2 + |Q_{e_R f_L}|^2}
\end{aligned} \tag{4.4}$$

for $\sqrt{s} \gg m_f$. In the SM, the forward-backward asymmetry $A_{FB}^{f\bar{f}}$ becomes constant for $\sqrt{s} \gg m_Z$. For $f\bar{f} = \mu^- \mu^+$, for instance, $A_{FB}^{\mu^- \mu^+}(P_{e^-}, P_{e^+}) \simeq 3/4$ at Z -pole $\sqrt{s} = m_Z$ since $|Q_{e_L \mu_L}| \gg |Q_{e_R \mu_L}|, |Q_{e_L \mu_R}|, |Q_{e_R \mu_L}|$, and $A_{FB}^{\mu^- \mu^+}(P_{e^-}, P_{e^+})$ approaches constant for $\sqrt{s} \gg m_Z$.

In the GHU (B) in Table 3, due to the interference effects between Z and Z' bosons, $|Q_{e_L \mu_L}|$ can be smaller than $|Q_{e_L \mu_R}|$ in some energy region (around $\sqrt{s} \sim 1.7$ TeV). Consequently $A_{FB}^{f\bar{f}}$ can become negative even for $\sqrt{s} \gg m_Z$ as shown in Figure 6. Deviation from the SM starts to show up around $\sqrt{s} = 250$ GeV. As shown in the middle and right columns in Figure 6, the amount of the deviation $\Delta_{FB}^{f\bar{f}}(P_{e^-}, P_{e^+} = 0)$ in Eq. (3.18) becomes significant for $P_{e^-} \sim -1$ even at $\sqrt{s} = 250$ GeV.

f	g_{Zf}^L	g_{Zf}^R	$g_{Z^{(1)}f}^L$	$g_{Z^{(1)}f}^R$	$g_{Z_R^{(1)}f}^L$	$g_{Z_R^{(1)}f}^R$	$g_{\gamma^{(1)}f}^L$	$g_{\gamma^{(1)}f}^R$
ν_e	0.5690	0	3.0096	0	-0.9511	0	0	0
ν_μ	0.5690	0	2.8509	0	-0.9039	0	0	0
ν_τ	0.5690	0	2.7412	0	-0.8712	0	0	0
e	-0.3059	0.2630	-1.6181	-0.0652	-0.9602	0	-2.5341	0.1194
μ	-0.3059	0.2630	-1.5328	-0.0652	-0.9125	0	-2.4004	0.1194
τ	-0.3059	0.2630	-1.4739	-0.0652	-0.8795	0.0001	-2.3080	0.1193
u	0.3936	-0.1754	2.0096	0.0435	0.3125	0	1.6306	-0.0796
c	0.3936	-0.1754	1.9260	0.0435	0.3003	0	1.5628	-0.0796
t	0.3940	-0.1750	1.4605	-0.3819	0.2318	-0.8528	1.1853	0.7016
d	-0.4813	0.0877	-2.4572	0.1237	0.3037	-0.1923	-0.8153	-0.2252
s	-0.4813	0.0877	-2.3551	0.1544	0.2919	-0.2327	-0.7814	-0.2810
b	-0.4813	0.0877	-1.7861	0.3075	0.2254	-0.4333	-0.5926	-0.5600

Table 8: Coupling constants of neutral vector bosons, Z' bosons, to fermions in units of $g_w = e/\sin\theta_W^0$ are listed for $\theta_H = 0.09$ and $m_{KK} = 13.00$ TeV (B^-) in Table 3, where $\sin^2\theta_W^0 = 0.2307$. Other information is the same as in Table 4.

4.4 Left-right asymmetry

The integrated left-right asymmetry in $e^-e^+ \rightarrow f\bar{f}$ ($f\bar{f} = \mu^-\mu^+, c\bar{c}, b\bar{b}, t\bar{t}$), $A_{LR}^{f\bar{f}}$, is shown in Figure 7. The integrated left-right asymmetry $A_{LR}^{f\bar{f}}$ in Eq. (3.25) is given by

$$A_{LR}^{f\bar{f}} \simeq \frac{[|Q_{e_L f_L}|^2 + |Q_{e_L f_R}|^2] - [|Q_{e_R f_R}|^2 + |Q_{e_R f_L}|^2]}{[|Q_{e_L f_L}|^2 + |Q_{e_L f_R}|^2] + [|Q_{e_R f_R}|^2 + |Q_{e_R f_L}|^2]} \quad (4.5)$$

for $m_f \ll \sqrt{s}$. In the center-of-mass energy region of interest $|Q_{e_L f_L}| \gg |Q_{e_L f_R}|$ and $|Q_{e_R f_R}| \gg |Q_{e_R f_L}|$ are satisfied so that

$$A_{LR}^{f\bar{f}} \simeq \frac{|Q_{e_L f_L}|^2 - |Q_{e_R f_R}|^2}{|Q_{e_L f_L}|^2 + |Q_{e_R f_R}|^2}. \quad (4.6)$$

In the GHU (B) in Table 3, due to the interference effects between Z and Z' bosons, $|Q_{e_L \mu_L}|$ becomes smaller than $|Q_{e_R \mu_R}|$ in the region around $\sqrt{s} = 1 \sim 2$ TeV as shown in Figure 4. Consequently $A_{LR}^{f\bar{f}}$ can be negative even for $\sqrt{s} \gg m_Z$.

The differential left-right asymmetry of $e^-e^+ \rightarrow f\bar{f}$ ($f\bar{f} = \mu^-\mu^+, c\bar{c}, b\bar{b}, t\bar{t}$), $A_{LR}^{f\bar{f}}(\cos\theta)$, is given by Eq. (3.20), and is displayed in Figure 8. In most of center-of-mass energy region of interest, relations $|Q_{e_L f_L}| \gg |Q_{e_L f_R}|$ and $|Q_{e_R f_R}| \gg |Q_{e_R f_L}|$ are satisfied so that in the forward region $\cos\theta > 0$, the differential left-right asymmetry is approximately

$$A_{LR}^{f\bar{f}}(\cos\theta) \simeq \frac{|Q_{e_L f_L}|^2 - |Q_{e_R f_R}|^2}{|Q_{e_L f_L}|^2 + |Q_{e_R f_R}|^2}. \quad (4.7)$$

k	$m_{Z^{(2k-1)}} [\text{TeV}]$	$g_{Z^{(2k-1)}e}^L$	$g_{Z^{(2k-1)}e}^R$	$m_{Z^{(2k)}} [\text{TeV}]$	$g_{Z^{(2k)}e}^L$	$g_{Z^{(2k)}e}^R$
1	10.20	-1.7621	-0.0584	15.86	-0.0064	-0.0040
2	23.09	-0.6931	0.0403	29.03	-0.0021	0.0030
3	36.07	-0.2514	-0.0329	42.10	-0.0010	-0.0025
4	49.06	-0.1480	0.0286	55.14	-0.0006	0.0022
5	62.05	-0.0882	-0.0257	68.16	-0.0004	-0.0020
6	75.05	-0.0626	0.0235	81.17	-0.0003	0.0018
7	88.05	-0.0443	-0.0219	94.18	-0.0002	-0.0017
8	101.0	-0.0344	0.0205	107.2	-0.0002	0.0016
9	114.0	-0.0265	-0.0194	120.2	-0.0001	-0.0015
10	127.0	-0.0217	0.0185	133.2	-0.0001	0.0015

k	$m_{Z_R^{(k)}} [\text{TeV}]$	$g_{Z_R^{(k)}e}^L$	$g_{Z_R^{(k)}e}^R$	$m_{\gamma^{(k)}} [\text{TeV}]$	$g_{\gamma^{(k)}e}^L$	$g_{\gamma^{(k)}e}^R$
1	9.951	-1.0444	0	10.20	-2.7587	0.1071
2	22.84	-0.4158	0	23.10	-1.0851	-0.0739
3	35.81	-0.1494	0	36.07	-0.3936	0.0603
4	48.79	-0.0877	0	49.06	-0.2318	-0.0524
5	61.78	-0.0521	0	62.05	-0.1380	0.0470
6	74.78	-0.0370	0	75.05	-0.0981	-0.0431
7	87.77	-0.0261	0	88.05	-0.0693	0.0401
8	100.8	-0.0203	0	101.0	-0.0539	-0.0376
9	113.8	-0.0156	0	114.0	-0.0415	0.0356
10	126.8	-0.0128	0	127.0	-0.0340	-0.0339

Table 9: Masses of neutral KK vector bosons $Z^{(2k-1)}$, $Z^{(2k)}$, $Z_R^{(k)}$, $\gamma^{(k)}$ ($k = 1, 2, \dots, 10$) and their couplings constants to left- and right-handed electrons in units of $g_w = e/\sin\theta_W^0$ are listed for $\theta_H = 0.10$ and $m_{\text{KK}} = 13.00$ TeV (B) in Table 3, where $\sin^2\theta_W^0 = 0.2306$. Other information is the same as in Table 4.

4.5 Left-right forward-backward asymmetry

The left-right forward-backward asymmetry $A_{LR,FB}^{f\bar{f}}(\cos\theta)$ is given by in Eq. (3.32). It is shown in Figure 9. For $|Q_{e_L f_L}| \gg |Q_{e_L f_R}|$, $|Q_{e_R f_R}| \gg |Q_{e_R f_L}|$ and $m_f \ll \sqrt{s}$, the left-right forward-backward asymmetry can be written in terms of the integrated left-right asymmetry $A_{LR}^{f\bar{f}}$ by

$$A_{LR,FB}^{f\bar{f}}(\cos\theta) \simeq \frac{2 \cos\theta}{1 + \cos^2\theta} \frac{|Q_{e_L f_L}|^2 - |Q_{e_R f_R}|^2}{|Q_{e_L f_L}|^2 + |Q_{e_R f_R}|^2} \simeq \frac{2 \cos\theta}{1 + \cos^2\theta} A_{LR}^{f\bar{f}}. \quad (4.8)$$

5 Summary and discussions

In the present paper, we evaluated total and differential cross sections, forward-backward asymmetries, differential and integrated left-right asymmetries, and left-right forward-backward asymmetries in the process $e^-e^+ \rightarrow f\bar{f}$ ($f\bar{f} = \mu^-\mu^+, c\bar{c}, b\bar{b}, t\bar{t}$) in the GUT

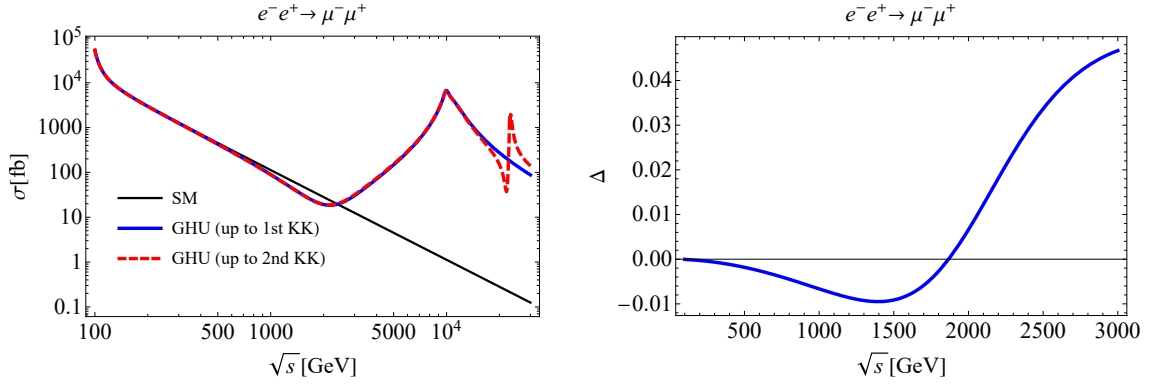


Figure 1: Total cross section $\sigma(e^-e^+ \rightarrow \mu^-\mu^+)$ with and without the contribution from the “second KK modes” ($\gamma^{(2)}, Z^{(2)}, Z^{(3)}, Z_R^{(2)}$) is shown. The left figure shows the total cross section $\sigma(e^-e^+ \rightarrow \mu^-\mu^+)$ with unpolarized electron and positron beams in the SM and the GHU (B) model in Table 3 up to $\sqrt{s} = 30$ TeV. The right figure shows the proportion of the contribution from the second KK modes, $\Delta = \sigma(\text{up to 2nd KK})/\sigma(\text{up to 1st KK}) - 1$. The contribution from the second KK modes remains small for $\sqrt{s} < 3$ TeV.

inspired GHU model. We showed that significant deviations in total cross sections from those in the SM can be detected even in the early stage of the ILC experiment at 250 GeV with $L_{\text{int}} = 250 \text{ fb}^{-1}$ data. By examining the dependence on the polarization of electrons and positrons, the two GHU models, the A- and B-models, can be distinguished up to $m_{\text{KK}} \simeq 15$ TeV. In differential cross sections and forward-backward asymmetry for $f\bar{f} = \mu^-\mu^+$ deviations from the SM are observed with the polarization $(P_{e^-}, P_{e^+}) = (-0.8, +0.3)$ and $m_{\text{KK}} \sim 10$ TeV. Deviations from the SM in the differential left-right asymmetry and the left-right forward-backward asymmetry for $f\bar{f} = \mu^-\mu^+$ are also observed with $m_{\text{KK}} \sim 10$ TeV. In these analyses we have checked that contributions from the second KK modes are negligible compared to those from the first KK modes in the energy region $\sqrt{s} \leq 1$ TeV.

The main reason for having these large effects lies in the fact that couplings of leptons and quarks to Z' bosons exhibit large parity violation. In the GUT inspired GHU (the B-model) left-handed leptons and light quarks have much larger couplings than right-handed ones as shown in Tables 4–8. The magnitudes of those left-handed couplings are much larger than those of the Z couplings. This is a special feature in GHU models formulated in the Randall-Sundrum (RS) warped space. KK gauge bosons in the RS space, including Z' bosons in our case, are localized near the IR brane at $z = z_L$. In GHU both left- and right-handed components of each lepton or quark are in one gauge multiplet, and each lepton or quark acquires a mass mainly through the Hosotani mechanism. It implies in the RS space that if the left-handed component is localized near the IR brane as in the B-model, then the right-handed component is localized near the UV brane, and the

left-handed component has a large coupling to Z' bosons as the overlap of wave functions becomes large.

There have been many GHU models formulated in flat space, particularly on $M^4 \times (S^1/Z_2)$ [86, 89–92]. In flat space Z' bosons are symmetrically distributed around the midpoint in the fifth dimension. In most cases leptons and quarks have uniform wave functions in the fifth dimension so that there arises no large parity violation in the Z' couplings. In some models on $M^4 \times (S^1/Z_2)$ additional kink-mass terms are introduced to make left-handed and right-handed components are localized near one brane or the other brane. Even in this case no large parity violation emerges in the Z' couplings as Z' bosons are symmetrically distributed in the fifth dimension.

In the composite Higgs model composite vector bosons play the role of Z' bosons [79]. It has been argued that the composite Higgs model is AdS dual of five-dimensional gauge theory [7]. In this picture Z' bosons correspond to KK gauge bosons as in GHU. In most of the composite Higgs models leptons and quarks except for the top quark are supposed to be localized near the UV brane so that they do not couple to Z' bosons very much. Except for the $e^-e^+ \rightarrow t\bar{t}$ process one does not expect significant deviations from the SM due to Z' bosons.

In the present paper, we focused on the analysis of the s -channel scattering processes $e^-e^+ \rightarrow f\bar{f}$ ($f\bar{f} \neq e^-e^+$) mediated by neutral vector bosons Z' in the GHU B-model. For $e^-e^+ \rightarrow e^-e^+$, there is a contribution not only from the s -channel scattering process but also from the t -channel scattering process. The formulas for several observables in the scattering process $e^-e^+ \rightarrow f\bar{f}$ in Sec. 3 need to be modified for $e^-e^+ \rightarrow e^-e^+$. It has been pointed out in Ref. [23] that for the scattering process $e^-e^+ \rightarrow e^-e^+$, deviations from the SM in the GHU A-model can be detected even in the early stage of the ILC experiment at 250 GeV, and therefore we expect similar deviations from the SM in the GHU B-model as well. We plan to give a detailed analysis of the $e^-e^+ \rightarrow e^-e^+$ scattering process in GHU in near future.

The scenario of gauge-Higgs unification (GHU) leads to distinct signals in electron-positron collision experiments. Clear deviations from the SM should be observed in the early stage of ILC 250 GeV experiments. In particular, GHU predicts strong dependence on the polarization of electron and positron beams, with which one can explore physics at the KK mass scale of 15 TeV.

Acknowledgments

This work was supported in part by European Regional Development Fund-Project Engineering Applications of Microworld Physics (No. CZ.02.1.01/0.0/0.0/16_019/0000766)

(Y.O.), by the National Natural Science Foundation of China (Grant Nos. 11775092, 11675061, 11521064, 11435003 and 11947213) (S.F.), by the International Postdoctoral Exchange Fellowship Program (IPEFP) (S.F.), and by Japan Society for the Promotion of Science, Grants-in-Aid for Scientific Research, No. 19K03873 (Y.H.) and Nos. 18H05543 and 19K23440 (N.Y.).

A Formulas of total and partial decay widths

We summarize formulas of total and partial decay widths of a vector boson in a tree-level approximation. The total decay width of a vector boson $\Gamma_{V'}$ is the sum of partial decay widths for all possible final states:

$$\Gamma_{V'} = \sum_{\sum_a m_{\chi_a} < m_{V'}} \Gamma(V' \rightarrow \prod_a \chi_a), \quad (\text{A.1})$$

where $\Gamma(V' \rightarrow \prod_a \chi_a)$ represents the partial decay width of V' to the final state $\prod_a \chi_a$. $m_{V'}$ and m_{χ_a} are masses of V' and χ_a , respectively.

In general, the partial decay width of V' to two particles $\chi_1 \chi_2$ is given by

$$\Gamma(V' \rightarrow \chi_1 \chi_2) = \frac{1}{16\pi m_{V'}} \sqrt{\lambda \left(1, \frac{m_{\chi_1}}{m_{V'}}, \frac{m_{\chi_2}}{m_{V'}} \right)} |\mathcal{M}_{\chi_1 \chi_2}|^2, \quad (\text{A.2})$$

$$\lambda(A, B, C) = A^4 + B^4 + C^4 - 2(A^2 B^2 + B^2 C^2 + C^2 A^2),$$

where m_{χ_i} ($i = 1, 2$) is the mass of the particle χ_j and $\mathcal{M}_{\chi_1 \chi_2}$ stands for the amplitude for $V' \rightarrow \chi_1 \chi_2$. For fermion final states $\chi_1 \chi_2 = f_1 f_2$

$$|\mathcal{M}_{f_1 f_2}|^2 = \frac{2}{3} N_c m_{V'}^2 \left\{ (g_L^2 + g_R^2) \left[1 - \frac{m_{f_1}^2 + m_{f_2}^2}{2m_{V'}^2} - \frac{(m_{f_1}^2 - m_{f_2}^2)^2}{2m_{V'}^4} \right] + 6g_L g_R \frac{m_{f_1} m_{f_2}}{m_{V'}^2} \right\}, \quad (\text{A.3})$$

where $g_{L/R}$ is the left- (right-)handed coupling constant of V' to f_1 and f_2 , and N_c is a color factor in the $SU(N_c)$ gauge group.

For $\chi_1 \chi_2 = V_1 V_2$ where V_1, V_2 are gauge bosons

$$|\mathcal{M}_{V_1 V_2}|^2 = \frac{1}{12} \frac{m_{V'}^6}{m_{f_1}^2 m_{f_2}^2} g_{V' V_1 V_2}^2 \left\{ \left(1 + \frac{m_{V_1}^4}{m_{V'}^4} + \frac{m_{V_2}^4}{m_{V'}^4} + 10 \frac{m_{V_1}^2 m_{V'}^2 + m_{V_2}^2 m_{V'}^2 + m_{V_1}^2 m_{V_2}^2}{m_{V'}^4} \right) \right. \\ \left. \times \left(1 - \frac{(m_{V_1} + m_{V_2})^2}{m_{V'}^2} \right) \left(1 - \frac{(m_{V_1} - m_{V_2})^2}{m_{V'}^2} \right) \right\}. \quad (\text{A.4})$$

Here m_{V_i} ($i = 1, 2$) is the mass of the gauge boson V_i , and $g_{V' V_1 V_2}$ is the coupling constant of V' to V_1 and V_2 . For $\chi_1 \chi_2 = V H$ where V and H are a gauge boson and scalar boson

$$|\mathcal{M}_{V H}|^2 = \frac{2}{3} g_{V' V H}^2 \left\{ \frac{(m_{V'}^2 + m_V^2 - m_H^2)^2}{8m_{V'}^2 m_V^2} + 1 \right\}, \quad (\text{A.5})$$

where m_V and m_H are the mass of the gauge boson V and the scalar H , respectively, and $g_{V'VH}$ is the coupling constant of V' to V and H . Normalization of $g_{V'V_1V_2}$ and $g_{V'VH}$ is given in Ref. [12].

References

- [1] Y. Hosotani, “Dynamical Mass Generation by Compact Extra Dimensions,” *Phys.Lett.* **B126** (1983) 309.
- [2] Y. Hosotani, “Dynamics of Nonintegrable Phases and Gauge Symmetry Breaking,” *Annals Phys.* **190** (1989) 233.
- [3] A. T. Davies and A. McLachlan, “Gauge Group Breaking By Wilson Loops,” *Phys. Lett.* **B200** (1988) 305.
- [4] A. T. Davies and A. McLachlan, “Congruency Class Effects in the Hosotani Model,” *Nucl. Phys.* **B317** (1989) 237.
- [5] H. Hatanaka, T. Inami, and C. S. Lim, “The Gauge Hierarchy Problem and Higher Dimensional Gauge Theories,” *Mod. Phys. Lett.* **A13** (1998) 2601–2612, [arXiv:hep-th/9805067](#).
- [6] H. Hatanaka, “Matter Representations and Gauge Symmetry Breaking via Compactified Space,” *Prog. Theor. Phys.* **102** (1999) 407–418, [arXiv:hep-th/9905100 \[hep-th\]](#).
- [7] K. Agashe, R. Contino, and A. Pomarol, “The Minimal Composite Higgs Model,” *Nucl. Phys.* **B719** (2005) 165–187, [arXiv:hep-ph/0412089 \[hep-ph\]](#).
- [8] A. D. Medina, N. R. Shah, and C. E. M. Wagner, “Gauge-Higgs Unification and Radiative Electroweak Symmetry Breaking in Warped Extra Dimensions,” *Phys. Rev.* **D76** (2007) 095010, [arXiv:0706.1281 \[hep-ph\]](#).
- [9] Y. Hosotani, K. Oda, T. Ohnuma, and Y. Sakamura, “Dynamical Electroweak Symmetry Breaking in $SO(5) \times U(1)$ Gauge-Higgs Unification with Top and Bottom Quarks,” *Phys.Rev.* **D78** (2008) 096002, [arXiv:0806.0480 \[hep-ph\]](#).
- [10] S. Funatsu, H. Hatanaka, Y. Hosotani, Y. Orikasa, and T. Shimotani, “Novel Universality and Higgs Decay $H \rightarrow \gamma\gamma$, gg in the $SO(5) \times U(1)$ Gauge-Higgs Unification,” *Phys. Lett.* **B722** (2013) 94–99, [arXiv:1301.1744 \[hep-ph\]](#).

- [11] S. Funatsu, H. Hatanaka, Y. Hosotani, Y. Orikasa, and T. Shimotani, “LHC Signals of the $SO(5) \times U(1)$ Gauge-Higgs Unification,” *Phys. Rev.* **D89** no. 9, (2014) 095019, [arXiv:1404.2748 \[hep-ph\]](#).
- [12] S. Funatsu, H. Hatanaka, Y. Hosotani, and Y. Orikasa, “Collider Signals of W' and Z' Bosons in the Gauge-Higgs Unification,” *Phys. Rev. D* **95** no. 3, (2017) 035032, [arXiv:1612.03378 \[hep-ph\]](#).
- [13] S. Funatsu, H. Hatanaka, Y. Hosotani, Y. Orikasa, and N. Yamatsu, “GUT Inspired $SO(5) \times U(1) \times SU(3)$ Gauge-Higgs Unification,” *Phys. Rev. D* **99** (2019) 095010, [arXiv:1902.01603 \[hep-ph\]](#).
- [14] S. Funatsu, H. Hatanaka, Y. Hosotani, Y. Orikasa, and N. Yamatsu, “CKM Matrix and FCNC Suppression in $SO(5) \times U(1) \times SU(3)$ Gauge-Higgs Unification,” *Phys. Rev. D* **101** (2020) 055016, [arXiv:1909.00190 \[hep-ph\]](#).
- [15] S. Funatsu, H. Hatanaka, Y. Hosotani, Y. Orikasa, and N. Yamatsu, “The Effective Potential and Universality in GUT Inspired Gauge-Higgs Unification,” To appear in *Phys. Rev. D* (2020) , [arXiv:2002.09262 \[hep-ph\]](#).
- [16] S. Funatsu, H. Hatanaka, and Y. Hosotani, “ $H \rightarrow Z\gamma$ in the Gauge-Higgs Unification,” *Phys. Rev.* **D92** (2015) 115003, [arXiv:1510.06550 \[hep-ph\]](#).
- [17] S. Funatsu, H. Hatanaka, Y. Hosotani, and Y. Orikasa, “Distinct Signals of the Gauge-Higgs Unification in e^+e^- Collider Experiments,” *Phys. Lett.* **B775** (2017) 297–302, [arXiv:1705.05282 \[hep-ph\]](#).
- [18] J. Yoon and M. E. Peskin, “Fermion Pair Production in $SO(5) \times U(1)$ Gauge-Higgs Unification Models,” [arXiv:1811.07877 \[hep-ph\]](#).
- [19] J. Yoon and M. E. Peskin, “Dissection of an $SO(5) \times U(1)$ Gauge-Higgs Unification Model,” *Phys. Rev.* **D100** no. 1, (2019) 015001, [arXiv:1810.12352 \[hep-ph\]](#).
- [20] S. Funatsu, “Forward-Backward Asymmetry in the Gauge-Higgs Unification at the International Linear Collider,” *Eur. Phys. J.* **C79** no. 10, (2019) 854, [arXiv:1905.10007 \[hep-ph\]](#).
- [21] Y. Hosotani, “Gauge-Higgs Unification at e^+e^- Linear Colliders,” *PoS CORFU2018* (2019) 075, [arXiv:1904.10156 \[hep-ph\]](#).
- [22] S. Bilokin, R. Pöschl, and F. Richard, “Measurement of b Quark EW Couplings at ILC,” [arXiv:1709.04289 \[hep-ex\]](#).

- [23] F. Richard, “Bhabha Scattering at ILC250,” [arXiv:1804.02846 \[hep-ex\]](#).
- [24] A. Irles, R. Pöschl, F. Richard, and H. Yamamoto, “Complementarity between ILC250 and ILC-GigaZ,” in *Linear Collider Community Meeting Lausanne, Switzerland*. 2019. [arXiv:1905.00220 \[hep-ex\]](#).
- [25] A. Irles, R. Pöschl, and F. Richard, “Production and Measurement of $e^+e^- \rightarrow c\bar{c}$ Signatures at the 250 GeV ILC,” in *International Workshop on Future Linear Colliders (LCWS 2019)*, Japan. 2019. [arXiv:2002.05805 \[hep-ex\]](#).
- [26] K. Fujii et al., “Physics Case for the 250 GeV Stage of the International Linear Collider,” [arXiv:1710.07621 \[hep-ex\]](#).
- [27] **ILC** Collaboration, H. Aihara et al., “The International Linear Collider. A Global Project,” [arXiv:1901.09829 \[hep-ex\]](#).
- [28] P. Bambade et al., “The International Linear Collider: A Global Project,” [arXiv:1903.01629 \[hep-ex\]](#).
- [29] T. Behnke, J. E. Brau, B. Foster, J. Fuster, M. Harrison, J. M. Paterson, M. Peskin, M. Stanitzki, N. Walker, and H. Yamamoto, “The International Linear Collider Technical Design Report - Volume 1: Executive Summary,” [arXiv:1306.6327 \[physics.acc-ph\]](#).
- [30] H. Baer, T. Barklow, K. Fujii, Y. Gao, A. Hoang, S. Kanemura, J. List, H. E. Logan, A. Nomerotski, M. Perelstein, et al., “The International Linear Collider Technical Design Report - Volume 2: Physics,” [arXiv:1306.6352 \[hep-ph\]](#).
- [31] C. Adolphsen, M. Barone, B. Barish, K. Buesser, P. Burrows, J. Carwardine, J. Clark, H. Mainaud Durand, G. Dugan, E. Elsen, et al., “The International Linear Collider Technical Design Report - Volume 3.I: Accelerator & in the Technical Design Phase,” [arXiv:1306.6353 \[physics.acc-ph\]](#).
- [32] C. Adolphsen, M. Barone, B. Barish, K. Buesser, P. Burrows, J. Carwardine, J. Clark, H. Mainaud Durand, G. Dugan, E. Elsen, et al., “The International Linear Collider Technical Design Report - Volume 3.II: Accelerator Baseline Design,” [arXiv:1306.6328 \[physics.acc-ph\]](#).
- [33] H. Abramowicz et al., “The International Linear Collider Technical Design Report - Volume 4: Detectors,” [arXiv:1306.6329 \[physics.ins-det\]](#).

- [34] G. Moortgat-Pick et al., “The Role of Polarized Positrons and Electrons in Revealing Fundamental Interactions at the Linear Collider,” *Phys. Rept.* **460** (2008) 131–243, [arXiv:hep-ph/0507011](#) [[hep-ph](#)].
- [35] Y. Hosotani and N. Yamatsu, “Gauge-Higgs Grand Unification,” *Prog. Theor. Exp. Phys.* **2015** (2015) 111B01, [arXiv:1504.03817](#) [[hep-ph](#)].
- [36] N. Yamatsu, “Gauge Coupling Unification in Gauge-Higgs Grand Unification,” *Prog. Theor. Exp. Phys.* **2016** (2016) 043B02, [arXiv:1512.05559](#) [[hep-ph](#)].
- [37] A. Furui, Y. Hosotani, and N. Yamatsu, “Toward Realistic Gauge-Higgs Grand Unification,” *Prog. Theor. Exp. Phys.* **2016** (2016) 093B01, [arXiv:1606.07222](#) [[hep-ph](#)].
- [38] Y. Hosotani, “New Dimensions from Gauge-Higgs Unification,” [arXiv:1702.08161](#) [[hep-ph](#)].
- [39] Y. Hosotani and N. Yamatsu, “Electroweak Symmetry Breaking and Mass Spectra in Six-Dimensional Gauge-Higgs Grand Unification,” *Prog. Theor. Exp. Phys.* **2018** no. 2, (2018) 023B05, [arXiv:1710.04811](#) [[hep-ph](#)].
- [40] Y. Hosotani and N. Yamatsu, “Gauge-Higgs Seesaw Mechanism in 6-Dimensional Grand Unification,” *Prog. Theor. Exp. Phys.* **2017** no. 9, (2017) 091B01, [arXiv:1706.03503](#) [[hep-ph](#)].
- [41] C. Englert, D. J. Miller, and D. D. Smaranda, “Phenomenology of GUT-Inspired Gauge-Higgs Unification,” *Phys. Lett. B* **802** (2020) 135261, [arXiv:1911.05527](#) [[hep-ph](#)].
- [42] C. Englert, D. J. Miller, and D. D. Smaranda, “The Weinberg Angle and 5D RGE Effects in a SO(11) GUT Theory,” *Phys. Lett. B* **807** (2020) 135548, [arXiv:2003.05743](#) [[hep-ph](#)].
- [43] H. Georgi and S. L. Glashow, “Unity of All Elementary Particle Forces,” *Phys. Rev. Lett.* **32** (1974) 438–441.
- [44] K. Inoue, A. Kakuto, and Y. Nakano, “Unification of the Lepton-Quark World by the Gauge Group SU(6),” *Prog. Theor. Phys.* **58** (1977) 630.
- [45] H. Fritzsch and P. Minkowski, “Unified Interactions of Leptons and Hadrons,” *Ann. Phys.* **93** (1975) 193–266.

- [46] F. Gursev, P. Ramond, and P. Sikivie, “A Universal Gauge Theory Model Based on E_6 ,” *Phys. Lett.* **B60** (1976) 177.
- [47] R. Slansky, “Group Theory for Unified Model Building,” *Phys. Rept.* **79** (1981) 1–128.
- [48] N. Yamatsu, “Finite-Dimensional Lie Algebras and Their Representations for Unified Model Building,” *arXiv:1511.08771* [hep-ph].
- [49] Y. Kawamura, “Gauge Symmetry Breaking from Extra Space S^1/Z_2 ,” *Prog. Theor. Phys.* **103** (2000) 613–619, *arXiv:hep-ph/9902423* [hep-ph].
- [50] Y. Kawamura, “Split Multiplets, Coupling Unification and Extra Dimension,” *Prog. Theor. Phys.* **105** (2001) 691–696, *arXiv:hep-ph/0012352*.
- [51] Y. Kawamura, “Triplet-Doublet Splitting, Proton Stability and Extra Dimension,” *Prog. Theor. Phys.* **105** (2001) 999–1006, *arXiv:hep-ph/0012125*.
- [52] G. Burdman and Y. Nomura, “Unification of Higgs and Gauge Fields in Five-Dimensions,” *Nucl. Phys.* **B656** (2003) 3–22, *arXiv:hep-ph/0210257* [hep-ph].
- [53] C. S. Lim and N. Maru, “Towards a Realistic Grand Gauge-Higgs Unification,” *Phys.Lett.* **B653** (2007) 320–324, *arXiv:0706.1397* [hep-ph].
- [54] K. Kojima, K. Takenaga, and T. Yamashita, “Grand Gauge-Higgs Unification,” *Phys. Rev.* **D84** (2011) 051701, *arXiv:1103.1234* [hep-ph].
- [55] K. Kojima, K. Takenaga, and T. Yamashita, “Gauge Symmetry Breaking Patterns in an SU(5) Grand Gauge-Higgs Unification Model,” *Phys. Rev.* **D95** no. 1, (2017) 015021, *arXiv:1608.05496* [hep-ph].
- [56] N. Yamatsu, “Special Grand Unification,” *Prog. Theor. Exp. Phys.* **2017** no. 6, (2017) 061B01, *arXiv:1704.08827* [hep-ph].
- [57] N. Yamatsu, “String-Inspired Special Grand Unification,” *Prog. Theor. Exp. Phys.* **2017** no. 10, (2017) 101B01, *arXiv:1708.02078* [hep-ph].
- [58] N. Yamatsu, “Family Unification in Special Grand Unification,” *Prog. Theor. Exp. Phys.* **2018** no. 9, (2018) 091B01, *arXiv:1807.10855* [hep-ph].
- [59] N. Maru and Y. Yatagai, “Fermion Mass Hierarchy in Grand Gauge-Higgs Unification,” *PTEP* **2019** no. 8, (2019) 083B03, *arXiv:1903.08359* [hep-ph].

- [60] B. Schrempp, F. Schrempp, N. Wermes, and D. Zeppenfeld, “Bounds on New Contact Interactions From Future e^+e^- Colliders,” Nucl. Phys. **B296** (1988) 1–25.
- [61] D. C. Kennedy, B. W. Lynn, C. J. C. Im, and R. G. Stuart, “Electroweak Cross-Sections and Asymmetries at the Z^0 ,” Nucl. Phys. **B321** (1989) 83–107.
- [62] **SLD** Collaboration, K. Abe et al., “Precise Measurement of the Left-Right Cross-Section Asymmetry in Z Boson Production by e^+e^- Collisions,” Phys. Rev. Lett. **73** (1994) 25–29, [arXiv:hep-ex/9404001 \[hep-ex\]](#).
- [63] **SLD** Collaboration, K. Abe et al., “An Improved Measurement of the Left-Right Z^0 Cross-Section Asymmetry,” Phys. Rev. Lett. **78** (1997) 2075–2079, [arXiv:hep-ex/9611011 \[hep-ex\]](#).
- [64] A. Blondel, B. W. Lynn, F. M. Renard, and C. Verzegnassi, “Precision Measurements of Final State Weak Coupling From Polarized Electron - Positron Annihilation,” Nucl. Phys. **B304** (1988) 438–450.
- [65] **SLD** Collaboration, K. Abe et al., “Measurement of A_b and A_c from the Left-Right Forward-Backward Asymmetry of Leptons in Hadronic Events at the Z^0 Resonance,” Phys. Rev. Lett. **74** (1995) 2895–2899.
- [66] **SLD** Collaboration, K. Abe et al., “Measurement of A_b from the Left-Right Forward-Backward Asymmetry of b Quark Production in Z^0 Decays Using a Momentum-Weighted Track-Charge Technique,” Phys. Rev. Lett. **74** (1995) 2890–2894.
- [67] **SLD** Collaboration, K. Abe et al., “Measurement of the Left-Right Forward-Backward Asymmetry for Charm Quarks with D^{*+} and D^+ Mesons,” Phys. Rev. Lett. **75** (1995) 3609–3613.
- [68] **SLD** Collaboration, K. Abe et al., “Polarized Bhabha Scattering a Precision Measurement of the Electron Neutral Current Couplings,” Phys. Rev. Lett. **74** (1995) 2880–2884, [arXiv:hep-ex/9410009 \[hep-ex\]](#).
- [69] **ALEPH, DELPHI, L3, OPAL, LEP Electroweak** Collaboration, S. Schael et al., “Electroweak Measurements in Electron-Positron Collisions at W-Boson-Pair Energies at LEP,” Phys. Rept. **532** (2013) 119–244, [arXiv:1302.3415 \[hep-ex\]](#).

- [70] D. Bardin, Y. Dydyshka, L. Kalinovskaya, L. Rumyantsev, A. Arbuzov, R. Sadykov, and S. Bondarenko, “One-Loop Electroweak Radiative Corrections to Polarized Bhabha Scattering,” *Phys. Rev.* **D98** no. 1, (2018) 013001, [arXiv:1801.00125 \[hep-ph\]](#).
- [71] V. I. Borodulin, R. N. Rogalyov, and S. R. Slabospitskii, “CORE 3.1 (Compendium of RElations, Version 3.1),” [arXiv:1702.08246 \[hep-ph\]](#).
- [72] P. Langacker, “The Physics of Heavy Z' Gauge Bosons,” *Rev. Mod. Phys.* **81** (2009) 1199–1228, [arXiv:0801.1345 \[hep-ph\]](#).
- [73] Y. Deguchi, H. Yamashiro, T. Suehara, T. Yoshioka, K. Fujii, and K. Kawagoe, “Study of Fermion Pair Events at the 250 GeV ILC,” in *International Workshop on Future Linear Colliders*. 2, 2019. [arXiv:1902.05245 \[hep-ex\]](#).
- [74] **LCC Physics Working Group** Collaboration, K. Fujii et al., “Tests of the Standard Model at the International Linear Collider,” [arXiv:1908.11299 \[hep-ex\]](#).
- [75] G. Cacciapaglia, C. Pica, and F. Sannino, “Fundamental Composite Dynamics: A Review,” [arXiv:2002.04914 \[hep-ph\]](#).
- [76] R. Contino, “The Higgs as a Composite Nambu-Goldstone Boson,” in *Theoretical Advanced Study Institute in Elementary Particle Physics: Physics of the Large and the Small*, pp. 235–306. 2011. [arXiv:1005.4269 \[hep-ph\]](#).
- [77] B. Bellazzini, C. Csaki, and J. Serra, “Composite Higgses,” *Eur. Phys. J. C* **74** no. 5, (2014) 2766, [arXiv:1401.2457 \[hep-ph\]](#).
- [78] G. Giudice, C. Grojean, A. Pomarol, and R. Rattazzi, “The Strongly-Interacting Light Higgs,” *JHEP* **06** (2007) 045, [arXiv:hep-ph/0703164](#).
- [79] B. Bellazzini, C. Csaki, J. Hubisz, J. Serra, and J. Terning, “Composite Higgs Sketch,” *JHEP* **11** (2012) 003, [arXiv:1205.4032 \[hep-ph\]](#).
- [80] **ALEPH** Collaboration, A. Collaboration, D. Collaboration, L. Collaboration, O. Collaboration, S. Collaboration, L. E. W. Group, S. E. Group, and S. H. F. Group, “Precision Electroweak Measurements on the Z Resonance,” *Phys. Rept.* **427** (2006) 257, [arXiv:hep-ex/0509008](#).
- [81] **Particle Data Group** Collaboration, M. Tanabashi et al., “Review of Particle Physics,” *Phys. Rev.* **D98** no. 3, (2018) 030001.

- [82] N. Cabibbo, “Unitary Symmetry and Leptonic Decays,” *Phys. Rev. Lett.* **10** (1963) 531–533.
- [83] M. Kobayashi and T. Maskawa, “CP Violation in the Renormalizable Theory of Weak Interaction,” *Prog. Theor. Phys.* **49** (1973) 652–657.
- [84] Z. Maki, M. Nakagawa, and S. Sakata, “Remarks on the Unified Model of Elementary Particles,” *Prog. Theor. Phys.* **28** (1962) 870–880.
- [85] G. Cacciapaglia, C. Csaki, J. Galloway, G. Marandella, J. Terning, and A. Weiler, “A GIM Mechanism from Extra Dimensions,” *JHEP* **04** (2008) 006, [arXiv:0709.1714 \[hep-ph\]](#).
- [86] Y. Adachi, N. Kurahashi, C. S. Lim, and N. Maru, “Flavor Mixing in Gauge-Higgs Unification,” *JHEP* **11** (2010) 150, [arXiv:1005.2455 \[hep-ph\]](#).
- [87] Y. Adachi, N. Kurahashi, C. S. Lim, and N. Maru, “ D^0 - \bar{D}^0 Mixing in Gauge-Higgs Unification,” *JHEP* **01** (2012) 047, [arXiv:1103.5980 \[hep-ph\]](#).
- [88] Y. Adachi, N. Kurahashi, N. Maru, and K. Tanabe, “ B^0 - \bar{B}^0 Mixing in Gauge-Higgs Unification,” *Phys. Rev. D* **85** (2012) 096001, [arXiv:1112.6062 \[hep-ph\]](#).
- [89] M. Kubo, C. S. Lim, and H. Yamashita, “The Hosotani Mechanism in Bulk Gauge Theories with an Orbifold Extra Space S^1/Z_2 ,” *Mod. Phys. Lett. A* **17** (2002) 2249–2264, [arXiv:hep-ph/0111327](#).
- [90] C. Csaki, C. Grojean, and H. Murayama, “Standard Model Higgs from Higher Dimensional Gauge Fields,” *Phys. Rev. D* **67** (2003) 085012, [arXiv:hep-ph/0210133](#).
- [91] C. A. Scrucca, M. Serone, and L. Silvestrini, “Electroweak Symmetry Breaking and Fermion Masses from Extra Dimensions,” *Nucl. Phys. B* **669** (2003) 128–158, [arXiv:hep-ph/0304220](#).
- [92] A. Abdalgabar, M. O. Khojali, A. S. Cornell, G. Cacciapaglia, and A. Deandrea, “Unification of Gauge and Yukawa Couplings,” *Phys. Lett. B* **776** (2018) 231–235, [arXiv:1706.02313 \[hep-ph\]](#).

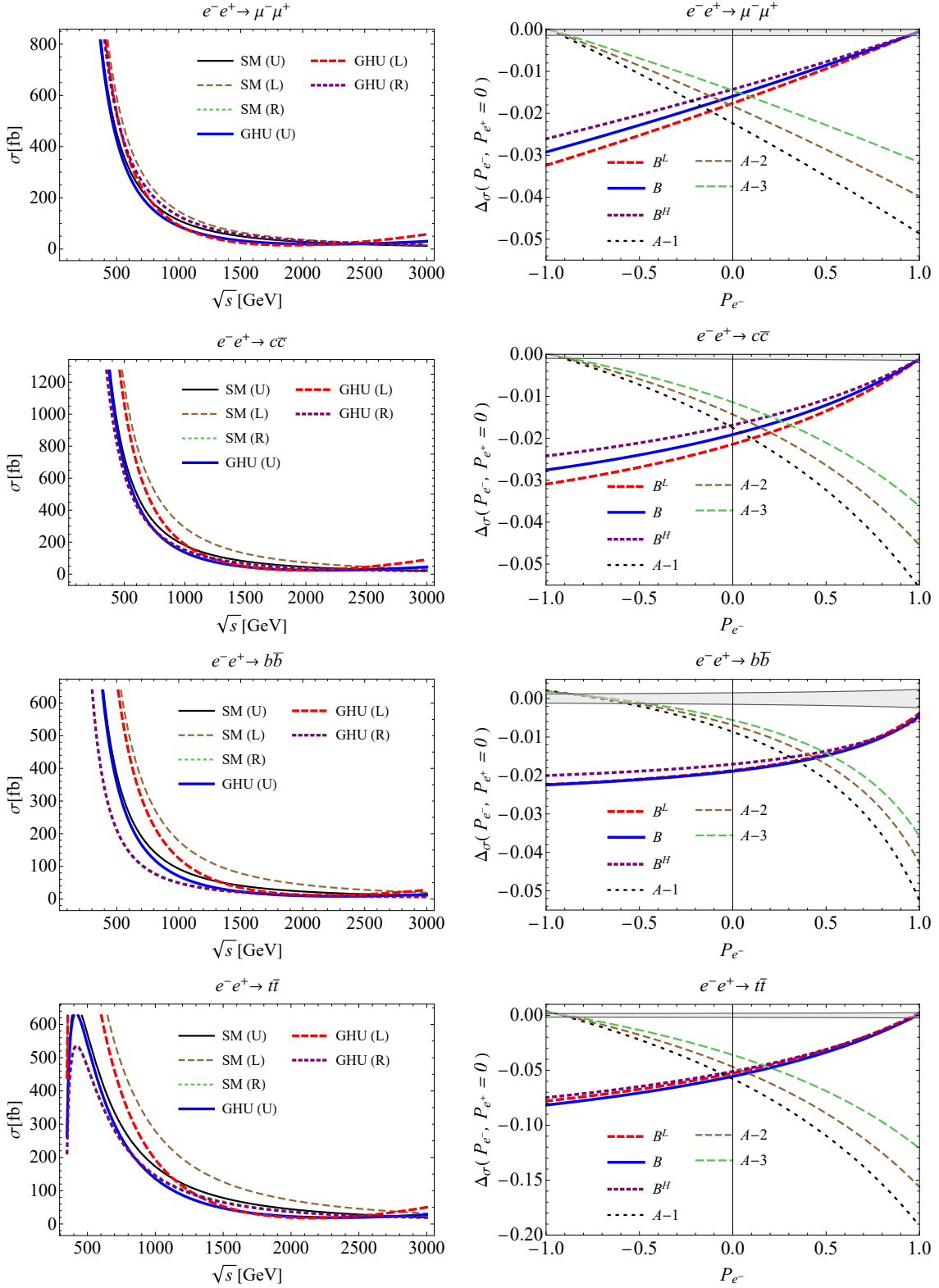


Figure 2: Total cross sections $\sigma^{f\bar{f}}$ ($f\bar{f} = \mu^-\mu^+, c\bar{c}, b\bar{b}, t\bar{t}$) are shown. On the left side the \sqrt{s} dependence of $\sigma^{f\bar{f}}$ in the SM and the GHU (B) in Table 3 with $(P_{e^-}, P_{e^+}) = (0, 0), (-0.8, +0.3), (+0.8, -0.3)$, which are referred to as (U), (L), (R), respectively, is shown. On the right side the electron polarization P_{e^-} dependence of the amount of the deviation from the SM, $\Delta_\sigma^{f\bar{f}}$ in Eq. (3.14), is shown for both the GUT (B -model) (B^L), (B), (B^H) and the previous GHU (A -model) ($\theta_H = 0.10, m_{KK} = 8.1 \text{ TeV}$), ($\theta_H = 0.09, m_{KK} = 8.7 \text{ TeV}$), ($\theta_H = 0.08, m_{KK} = 9.5 \text{ TeV}$) which are referred to as $A-1$, $A-2$ and $A-3$, respectively. The gray band represents the statistical error in the SM at $\sqrt{s} = 250 \text{ GeV}$ with 250 fb^{-1} data for $P_{e^-} = P_{e^+} = 0$. For the A -model, the masses and decay widths of the KK bosons and the coupling constants are listed in Ref. [17].

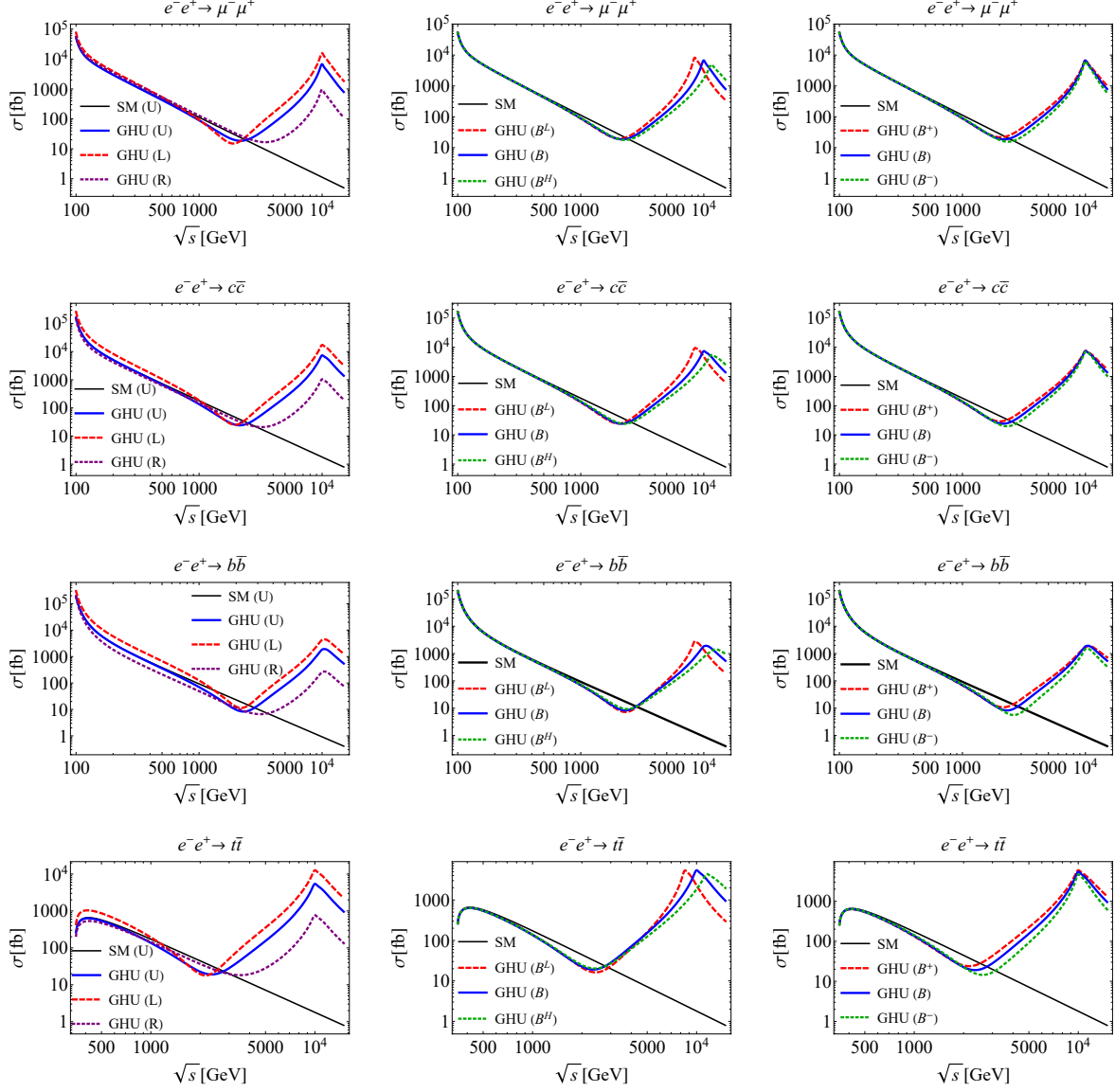


Figure 3: Total cross sections $\sigma^{f\bar{f}}$ ($f\bar{f} = \mu^-\mu^+, c\bar{c}, b\bar{b}, t\bar{t}$) are displayed in wider range of \sqrt{s} . In the left column $\sigma^{f\bar{f}}$ in GHU (B) is shown with polarized and unpolarized e^\pm beams with $(P_{e^-}, P_{e^+}) = (0, 0), (-0.8, +0.3), (+0.8, -0.3)$ which are referred to as (U), (L), (R), respectively. In the middle and right columns $\sigma^{f\bar{f}}$ with $(P_{e^-}, P_{e^+}) = (0, 0)$ is shown in the GHU (B^L), (B), (B^H) and in the GHU (B^+), (B), (B^-) in Table 3.

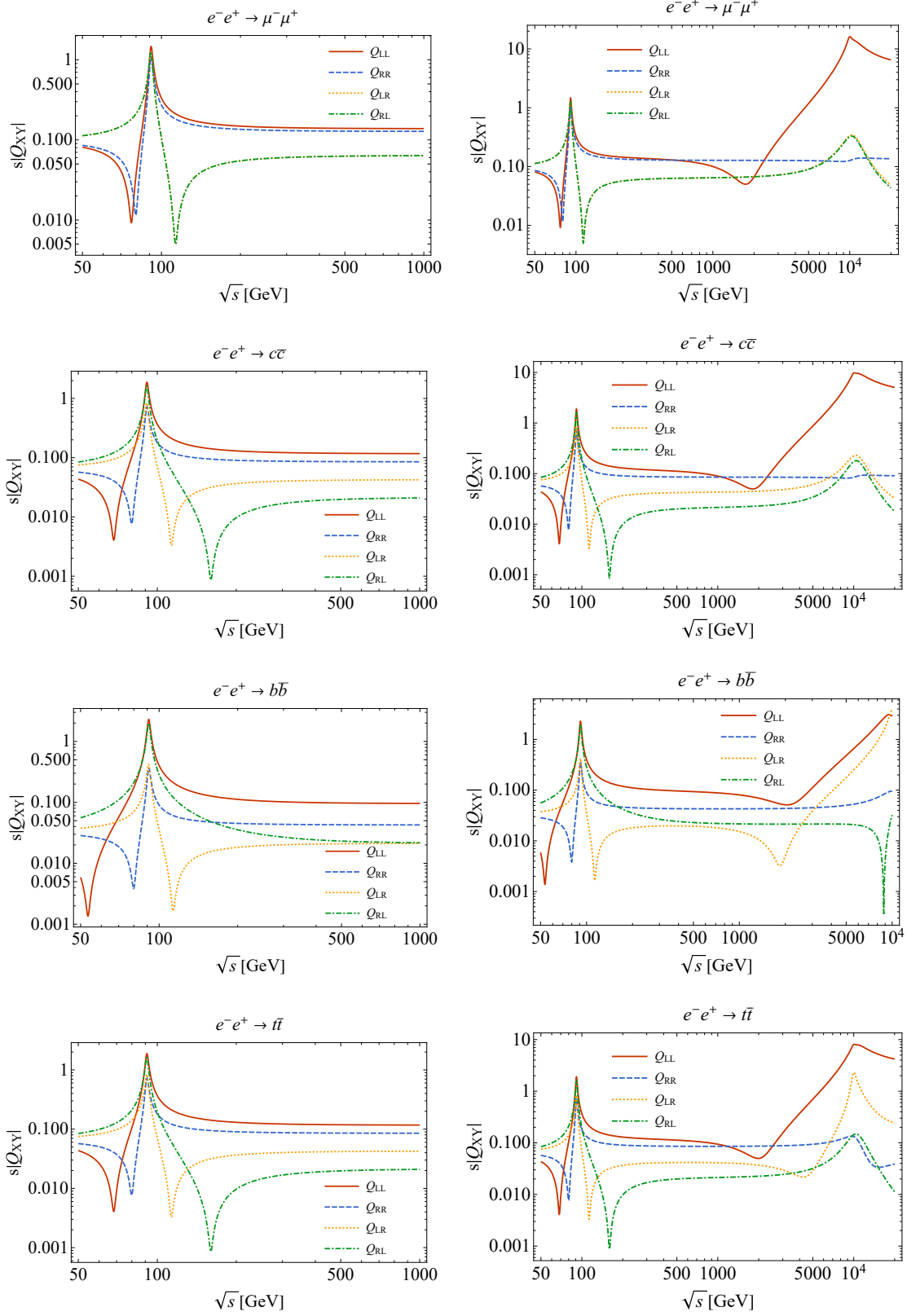


Figure 4: The amplitude $s|Q_{e_X f_Y}|(e^-e^+ \rightarrow f\bar{f})$ ($X, Y = L, R; f\bar{f} = \mu^-\mu^+, c\bar{c}, b\bar{b}, t\bar{t}$) vs \sqrt{s} [GeV] for the SM (left side figures) and the GHU (B) (right side figures) in Table 3 are shown. In each figure $Q_{e_X f_Y}$ is denoted as Q_{XY} . The energy ranges \sqrt{s} in the left and right side figures are $\sqrt{s} = [50, 1000]$ GeV and $\sqrt{s} = [50, 2 \times 10^4]$ GeV, respectively.

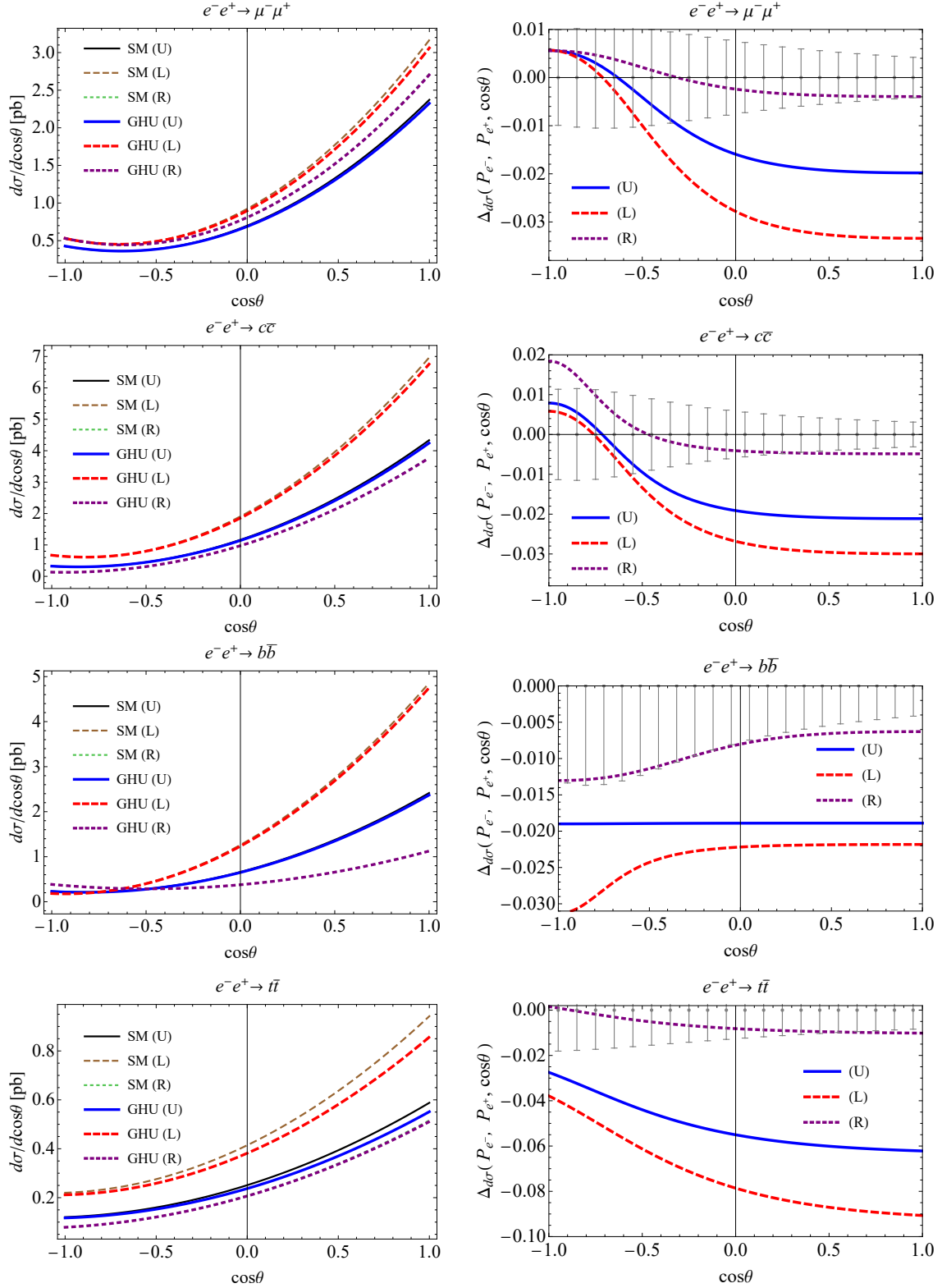


Figure 5: Differential cross sections $d\sigma^{f\bar{f}}/d\cos\theta$ ($f\bar{f} = \mu^-\mu^+, c\bar{c}, b\bar{b}, t\bar{t}$) are shown. The left side figures show the θ dependence of $d\sigma^{f\bar{f}}/d\cos\theta$ in the SM and the GHU (B) in Table 3 with three sets $(P_{e-}, P_{e+}) = (0, 0)(U), (-0.8, +0.3)(L), (+0.8, -0.3)(R)$. $\sqrt{s} = 250$ GeV for $f\bar{f} = \mu^-\mu^+, c\bar{c}, b\bar{b}$, and $\sqrt{s} = 500$ GeV for $f\bar{f} = t\bar{t}$. The right side figures show the θ dependence of $\Delta_{d\sigma}^{f\bar{f}}(P_{e-}, P_{e+}, \cos\theta)$ in (3.13). The error bars represent statistical errors in the SM at $\sqrt{s} = 250$ GeV with 250 fb^{-1} data for $f\bar{f} = \mu^-\mu^+, c\bar{c}, b\bar{b}$ and at $\sqrt{s} = 500$ GeV with 500 fb^{-1} data for $f\bar{f} = t\bar{t}$. Each bin is given by $\cos\theta = [k - 0.05, k + 0.05]$ ($k = -0.95, -0.85, \dots, 0.95$).

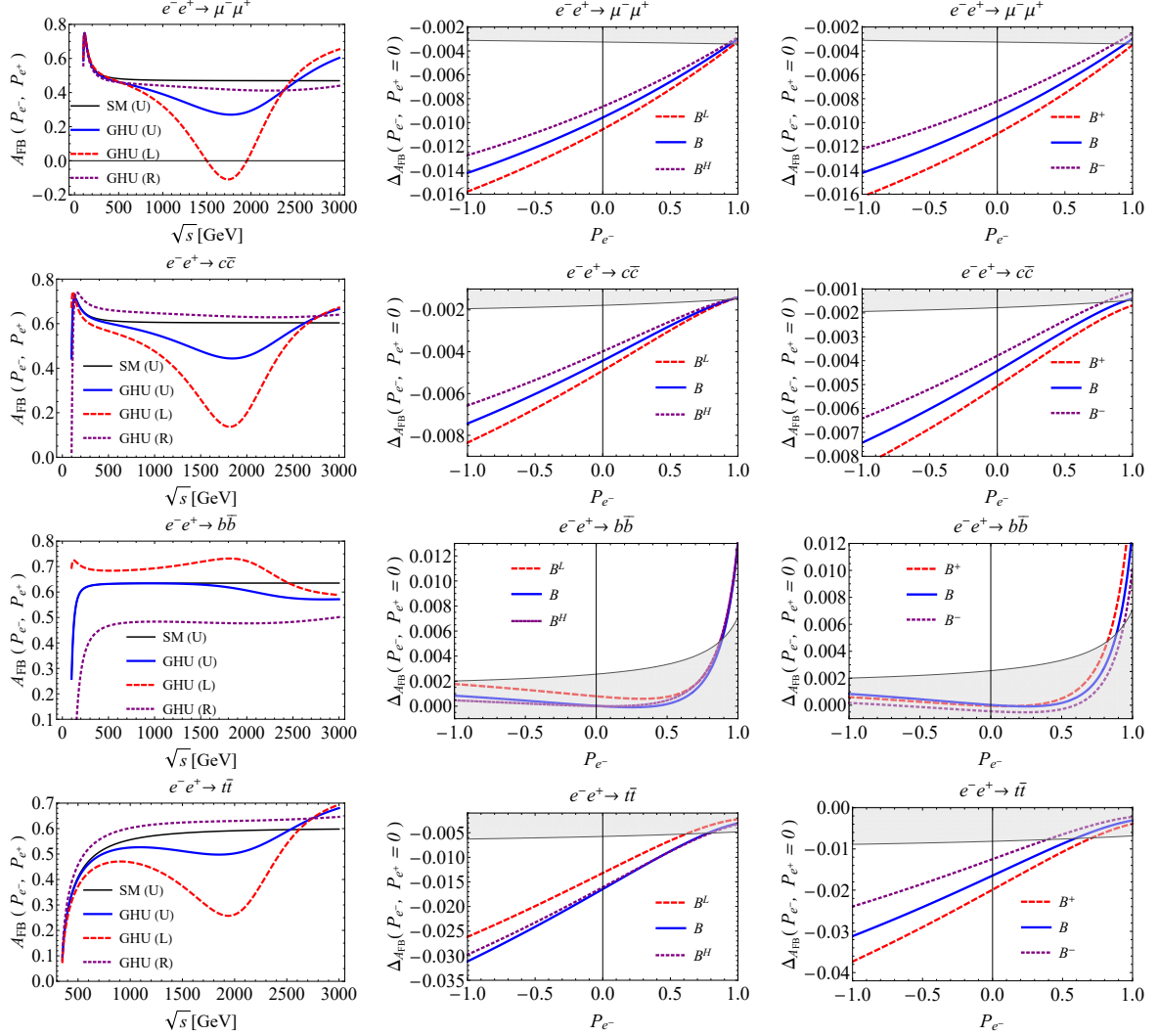


Figure 6: Forward-backward asymmetries $A_{FB}^{f\bar{f}}$ ($f\bar{f} = \mu^-\mu^+, c\bar{c}, b\bar{b}, t\bar{t}$) are shown. The left side figures show the \sqrt{s} dependence of $A_{FB}^{f\bar{f}}$ in the SM and the GHU (B) in Table 3. Three cases of polarization of electron and positron beams $(P_{e^-}, P_{e^+}) = (0, 0)(U), (-0.8, +0.3)(L), (+0.8, -0.3)(R)$ are depicted for GHU. The energy range \sqrt{s} is $[80, 3000]$ GeV for $f\bar{f} = \mu^-\mu^+, c\bar{c}, b\bar{b}$ and $[350, 3000]$ GeV for $f\bar{f} = t\bar{t}$. The central figures show the electron polarization P_{e^-} dependence of the deviation from the SM $\Delta_{A_{FB}}^{f\bar{f}}(P_{e^-}, P_{e^+} = 0)$ in Eq. (3.18) for the GHU (B^L), (B), (B^H) in Table 3. The right side figures show the electron polarization P_{e^-} dependence of the deviation for the GHU (B^+), (B), (B^-) in Table 3. The gray band in the central and right side figures represent the statistical error in the SM at $\sqrt{s} = 250$ GeV with 250 fb^{-1} data for $f\bar{f} = \mu^-\mu^+, c\bar{c}, b\bar{b}$ and at $\sqrt{s} = 500$ GeV with 500 fb^{-1} data for $f\bar{f} = t\bar{t}$.

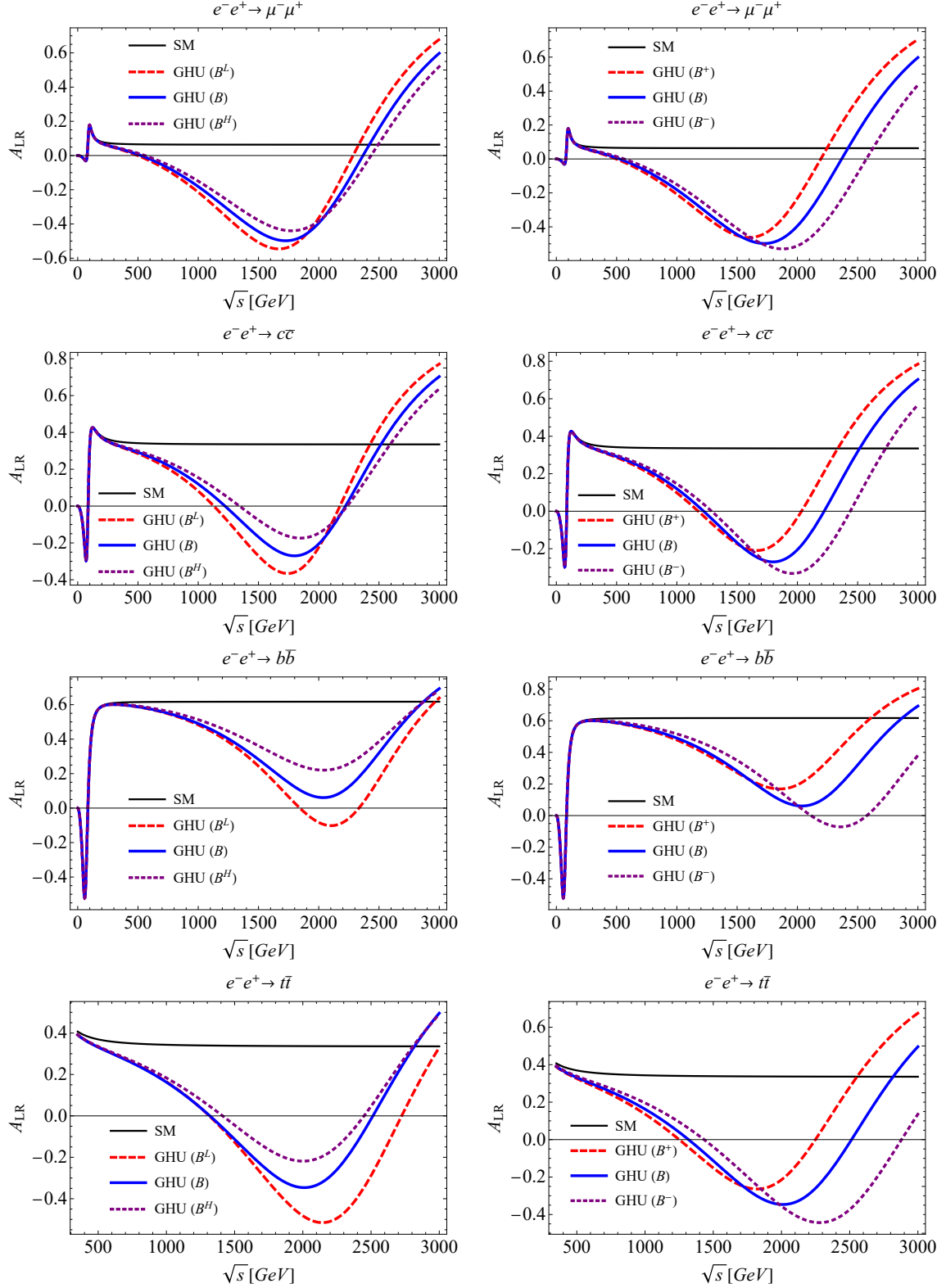


Figure 7: Left-right asymmetries $A_{LR}^{f\bar{f}}$ ($f\bar{f} = \mu^-\mu^+, c\bar{c}, b\bar{b}, t\bar{t}$) are shown. The left and right side figures show the \sqrt{s} dependence of the left-right asymmetry $A_{LR}^{f\bar{f}}$ for the SM and the GHU (B^L), (B), (B^H) and for the SM and the GHU (B^+), (B), (B^-) in Table 3. The energy ranges \sqrt{s} in the above figures are $[80, 3000]$ GeV and $[350, 3000]$ GeV for $f\bar{f} = \mu^-\mu^+, c\bar{c}, b\bar{b}$ and for $f\bar{f} = t\bar{t}$, respectively.

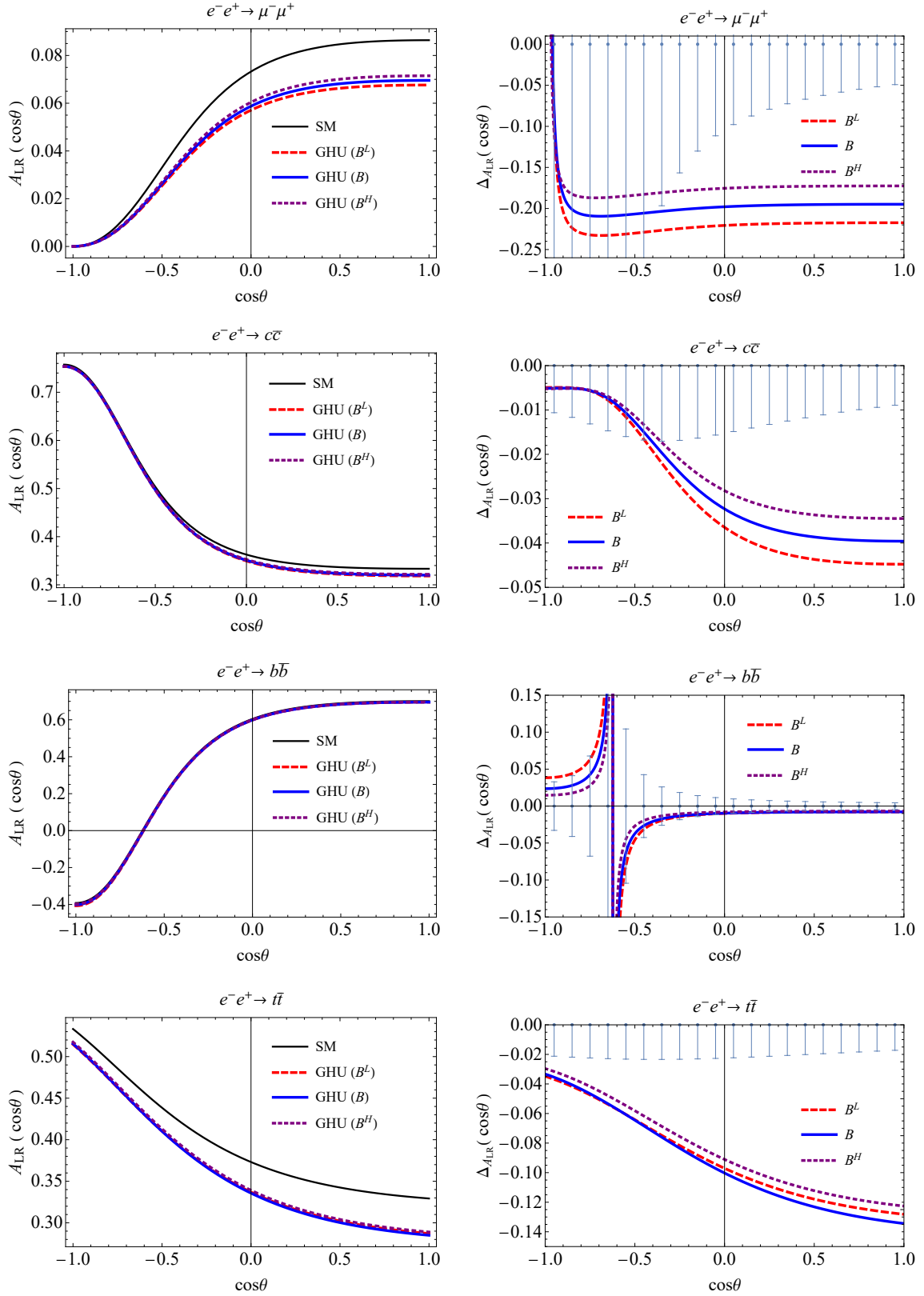


Figure 8: Differential left-right asymmetries $A_{LR}^{f\bar{f}}(\cos\theta)$ ($f\bar{f} = \mu^-\mu^+, c\bar{c}, b\bar{b}, t\bar{t}$) are shown. The left side figures show the θ dependence of $A_{LR}^{f\bar{f}}(\cos\theta)$ for the SM and the GHU (B^L), (B), (B^H) in Table 3. The right side figures show the θ dependence of the deviation of the differential left-right asymmetry from the SM, $\Delta A_{LR}^{f\bar{f}}(\cos\theta)$ in Eq. (3.29) for the GHU (B^L), (B), (B^H). The error bars in the right side figures represent the statistical error in Eq. (3.28) at $\sqrt{s} = 250$ GeV with 250 fb^{-1} data and $(P_{e^-}, P_{e^+}) = (-0.8, +0.3), (+0.8, -0.3)$ for $f\bar{f} = \mu^-\mu^+, c\bar{c}, b\bar{b}$ and at $\sqrt{s} = 500$ GeV with 500 fb^{-1} data for $f\bar{f} = t\bar{t}$.

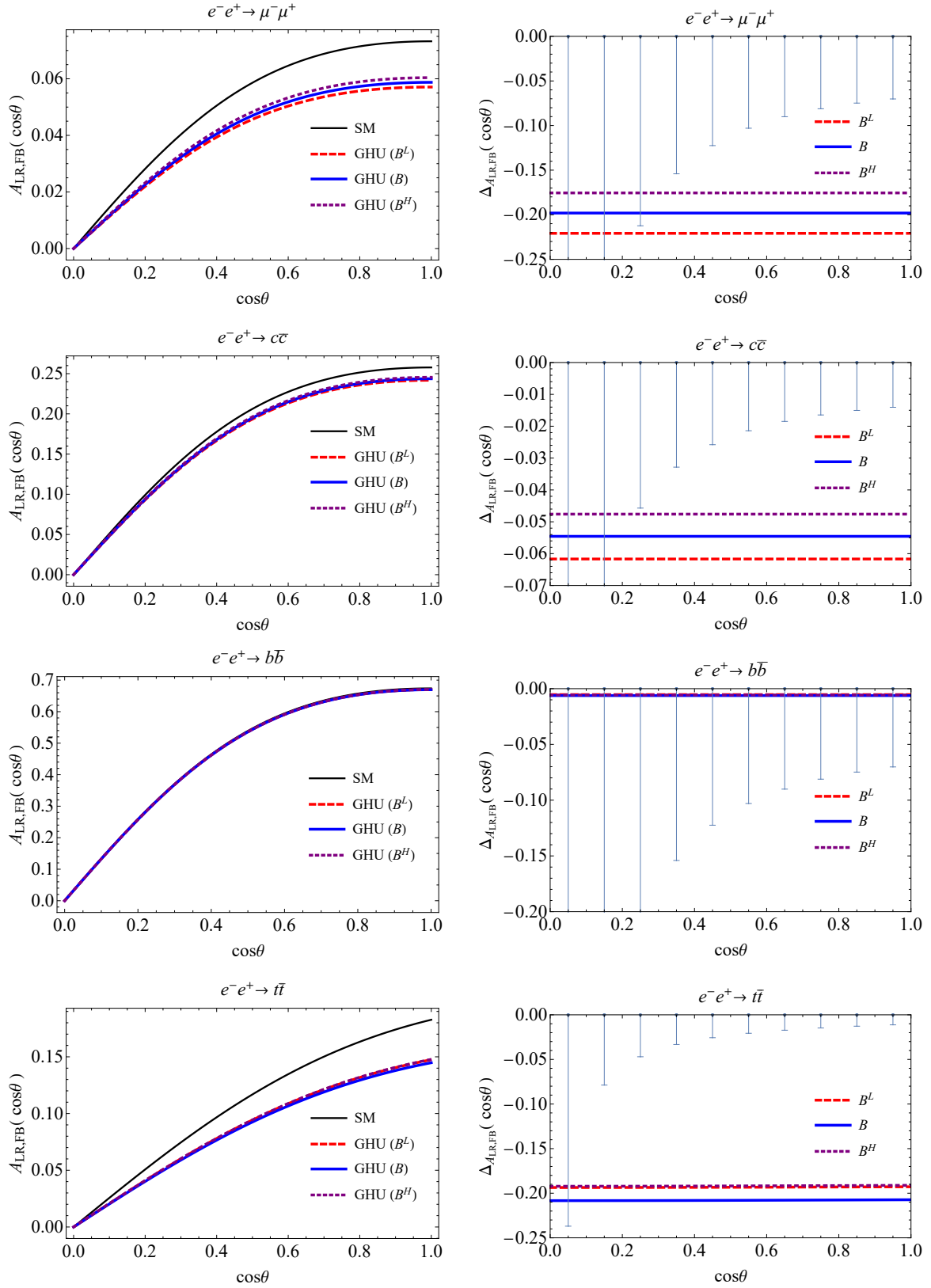


Figure 9: Left-right forward-backward asymmetries $A_{LR,FB}^{f\bar{f}}(\cos\theta)$ ($f\bar{f} = \mu^-\mu^+, c\bar{c}, b\bar{b}, t\bar{t}$) are shown. The left side figures show the \sqrt{s} dependence of $A_{LR,FB}^{f\bar{f}}(\cos\theta)$ for the SM and the GHU (B^L), (B), (B^H) in Table 3. The right figure shows the $\cos\theta$ dependence of the deviation of the left-right asymmetry from the SM, $\Delta A_{LR,FB}(\cos\theta)$ in Eq. (3.36) for the GHU (B^L), (B), (B^H) in Table 3. The error bars in the right side figures stand for the statistical error in Eq. (3.28) at $\sqrt{s} = 250$ GeV with 250 fb^{-1} data and $(P_{e^-}, P_{e^+}) = (-0.8, +0.3), (+0.8, -0.3)$ for $f\bar{f} = \mu^-\mu^+, c\bar{c}, b\bar{b}$ and at $\sqrt{s} = 500$ GeV with 500 fb^{-1} data for $f\bar{f} = t\bar{t}$.